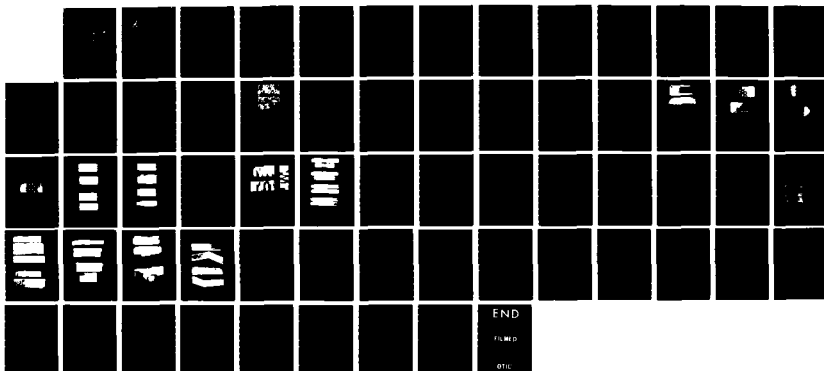DEVELOPMENT AND CHARACTERIZATION OF MULTILAYER
INTEGRATED WARHEAD STRUCTURE(U) ETA CORP ORANGE CA
D L MYKKANEN MAY 85 AMMRC-TR-85-10 DAAG46-83-C-0167

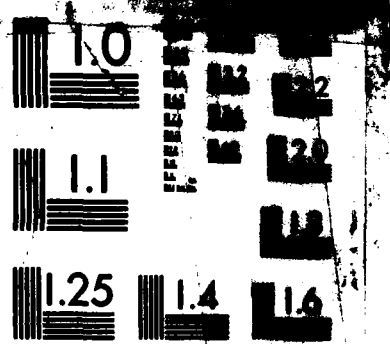UNCLASSIFIED

F/G 19/1

NL

END
FILMED

DTIC

MICROCOPY RESOLUTION TEST CHART

NATIONAL BUREAU OF STANDARDS-1963-A

AD-A157 946

AMMRC TR 85-10

DEVELOPMENT AND CHARACTERIZATION OF MULTILAYER
INTEGRATED WARHEAD STRUCTURE

May 1985

D. L. MYKKANEN
ETA CORPORATION
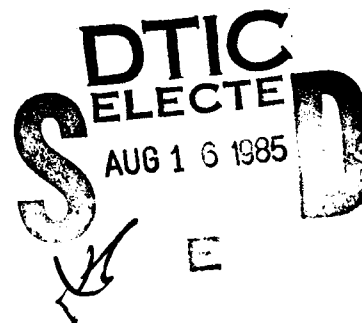P.O. Box 6625
Orange, California 92667

FINAL REPORT   Contract No. DAAG46-83-C-0167

DTIC FILE COPY

DTIC
ELECTE
AUG 1 6 1985
E

Prepared for

ARMY MATERIALS AND MECHANICS RESEARCH CENTER
Watertown, Massachusetts 02172-0001

85   812   011

REPORT DOCUMENTATION PAGE	READ INSTRUCTIONS BEFORE COMPLETING FORM

1. REPORT NUMBER	2. GOVT ACCESSION NO.	3. RECIPIENT'S CATALOG NUMBER
AMMRC TR 85-10	AD-A157946	

4. TITLE *(and Subtitle)*	5. TYPE OF REPORT & PERIOD COVERED
DEVELOPMENT AND CHARACTERIZATION OF MULTILAYER INTEGRATED WARHEAD STRUCTURE	Final Report 3/17/83 to 9/30/84
	6. PERFORMING ORG. REPORT NUMBER

7. AUTHOR(s)	8. CONTRACT OR GRANT NUMBER(s)
D. L. Mykkanen	DAAG46-83-C-0167

9. PERFORMING ORGANIZATION NAME AND ADDRESS	10. PROGRAM ELEMENT, PROJECT, TASK AREA & WORK UNIT NUMBERS
ETA CORPORATION P.O. Box 6625 Orange, CA 92667	D/A Project: 8X363304D215 AMCMS CODE: P693000.215

11. CONTROLLING OFFICE NAME AND ADDRESS	12. REPORT DATE
Army Materials and Mechanics Research Center ATTN: AMXMR-K Watertown, Massachusetts 02172-0001	May 1985
	13. NUMBER OF PAGES
	58

14. MONITORING AGENCY NAME & ADDRESS(*if different from Controlling Office*)	15. SECURITY CLASS. *(of this report)*
	Unclassified
	15a. DECLASSIFICATION/DOWNGRADING SCHEDULE

16. DISTRIBUTION STATEMENT *(of this Report)*

Approved for public release; distribution unlimited.

17. DISTRIBUTION STATEMENT *(of the abstract entered in Block 20, if different from Report)*

18. SUPPLEMENTARY NOTES

19. KEY WORDS *(Continue on reverse side if necessary and identify by block number)*

Warheads
Fragmentation
Investment casting

Tensile strength
Structural elements

20. ABSTRACT *(Continue on reverse side if necessary and identify by block number)*

(SEE REVERSE SIDE)

DD _{1 JAN 73} **1473** EDITION OF 1 NOV 65 IS OBSOLETE

Block No. 20

ABSTRACT

This experimental program demonstrated the potential benefits from an integrated multilayered fragmenting warhead structure which uses the structural weight as deliverable fragment mass and the fragment mass to increase the structural strength and stiffness. The fabrication techniques and design developments were accomplished using wax and polyester as surrogates for the ceramic cores and cast steel of the final concept. Steel castings (17-4PH) were made and specimens were machined to characterize the structural properties of the concept. The property measurements showed tensile strengths approaching the maximum possible for an annealed cast steel skin. The compressive strengths were greater than that expected for the skin membrane of the integrated structure. In flexure, the multilayer fragments construction was equivalent to a solid beam (on a per unit length basis) 70% the thickness of fragment structure. The shear banding found in the tensile specimens suggests a potential for fragmentation under explosive loading and justifies continuing to characterize the concept.
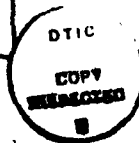
FORWARD

Accession For		
NTIS GRA&I	☒	
DTIC TAB	☐	
Unannounced	☐	
Justification		
By		
Distribution/		
Availability Codes		
Dist	Avail and/or Special	
A-1		

TABLE OF CONTENTS

ILLUSTRATIONS

LIST OF TABLES

1.0 INTRODUCTION

1.1 Background

In the past, conventional nonnuclear warheads for strategic defense systems have been contained as a separate subsystem within the warhead section. The warhead fragments are then explosively driven through the interceptor structure and heatshield toward the target. These separate systems result in a weight and performance penalty. The interceptor structural subsystem must be designed for minimum weight to efficiently survive the launch flight and blast environments while the warhead subsystem is designed for maximum fragment weight. Even with efficient design the structure is a weight penalty for the warhead. Combining the two subsystems achieves a system improvement. The structural design can incorporate enhanced stiffness and strength with no weight penalty. The fragments do not give up their kinetic energy penetrating the interceptor structure. In addition, the synergy allows for the original weight allotted to the structure to be included in the warhead, further increasing the total system performance.

Current concepts for NNK (Non Nuclear Kill) weapons without individual aiming are limited to essentially chunky fragments which when exploded are found in a mono-layer expanding cloud of fragments in flight. Penetration and internal damage would be enhanced if the fragment impacts are closely spaced causing interactions, such as side by side hits with interconnecting failures or if one wave of fragments penetrates the surface followed by a second wave of fragments which damage the internal structure. These benefits require either more accuracy for smaller miss distances or multiple layers of fragments with the same trajectory and close spacing in the fragment cloud.

These improvements can be achieved by creating a multi-layer cloud of fragments (possibly multiple layers) expanding from the exploded warhead. NNK single layered warheads would be improved if multiple layers were used to achieve closer spacing within the fragment cloud. In seeking an efficient method of stacking multiple layers of fragments the approaches used by nature were investigated. The most densely packed arrangement of geometric structures found in nature is a combination of tetrahedra and octahedra as shown in Figure 1.1. In crystalline structures these are called close-packed hexagonal or face centered cubic.

1

This construction of tetrahedra and octahedra has interesting characteristics. The tetrahedron is a minimum volume or mass unit cell with a maximum number of edges and corners. Structurally, its edges are ideally the most stable minimum mass truss construction. The tetrahedron can be considered to be the "sharpest" chunky fragment possible. The octahedron in the structure contains eight sides, each of which is the triangle, and four times the volume or mass of four-sided tetrahedron. The octahedron thus is a more massive and rounded chunky fragment. These two geometric natural structures can be fabricated as fragments by creating a skin or separation plane on one or both of the geometric volumes. In addition, since it is desired that the fragments have the same mass, the octahedron can be divided into subunits having the same mass as the tetrahedron with a portion of the octahedral volume used as separation plane or skin.

**OCTAHEDRA
FIT TETRAHEDRA**

**TETRAHEDRA
FIT OCTAHEDRA**
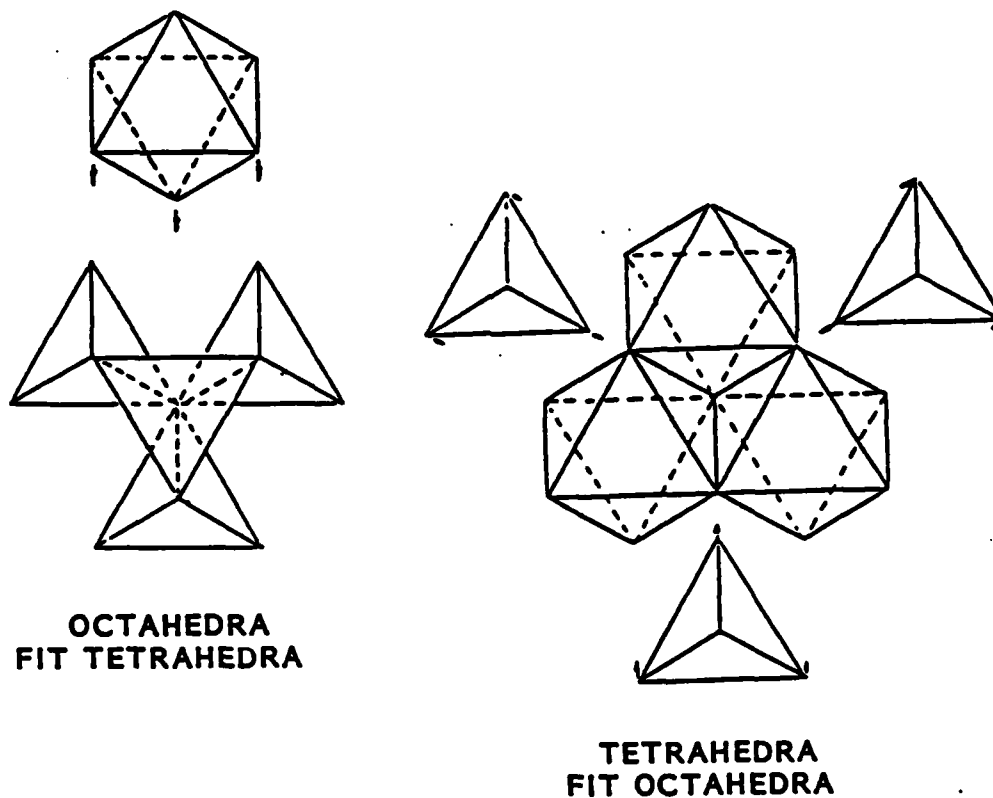
Figure 1.1 GEOMETRIC STRUCTURES

2

1.2 Program Technical Objectives

This program was carried out to demonstrate the feasibility of this unique multilayer fragmenting structural concept. The demonstration was planned as an experimental and analytical program. The mechanical properties predicted by the analytical model were to be compared with the measurement of these properties. The experimental results would be used to establish the feasibility.

In order to accomplish a lower cost development the early tests were to be carried out using substitute or surrogate materials. The surrogate materials development program provided low cost guidance for the tooling design and casting approaches for the final steel castings. When the surrogate manufacturing processes and procedures were evaluated and the surrogate composite properties measured, the final high temperature investment casting development efforts and property measurements would be accomplished using a high strength castable stainless steel. Casting and characterizing the steel concepts would demonstrate the structural properties of the integrated fragmenting warhead concept and provide direction for future efforts.

2.0 DESIGN DEVELOPMENT TASKS

2.1 Preliminary Development Tests

The preliminary development work was accomplished using surrogate materials and processes to carry out the casting studies.

2.1.1. Surrogate Materials Development

These original surrogate materials selected were a castable polyester resin to represent the steel, investment casting wax to represent the ceramic cores. The wax used as a surrogate-ceramic is the same type of wax which will be used later in the lost wax (investment casting) process for the steel castings. However, a special blend was used as the surrogate. The normal mechanical problems of an experimental program have been encountered with the addition of some unexpected problems with the surrogates.

2.1.1.1 Wax Development Problem

It was necessary to blend raw stock waxes into a special wax to be used as a surrogate. This was necessary to achieve the needed combination of shrinkage and handlability. Early attempts to cast wax cores meet with difficulties. The wax cores shrank onto their internal tooling core when solidifying. When the shrinkage is too great, the wax surrogate of the ceramic core would crack. When the shrinkage was sufficiently low to eliminate cracking, the wax did not have sufficient handlability to assemble into a core assembly. The development program first attempted to select from available commercial waxes. The parameters involved in the selection were shrinkage and resilience. Waxes were found which had sufficient resilience and low shrinkage such that they could be cast to represent the ceramic cores. These waxes commercially available for the investment (lost wax) foundry community are pigmented by the wax vendors for differentiation in the mold room . However, when these waxes were exposed to the liquid polyester resin the pigment leached from the wax coloring the resin and possibly changing the resin's cured properties. A number of vendors and a large series of the waxes were investigated. All exhibited the resin discoloring problem and it was necessary to develop a special pigment free wax. Non-pigmented raw stock waxes are available as "hard" (low shrinkage) and "soft" (high shrinkage) starting materials.

These were purchased and were blended to achieve a wax which when cast would have an acceptable combination of shrinkage and resilience to produce a usable core. The blend finally selected consisted of 60% "soft" and 40% "hard". This produced cores which had a minimum shrinkage cracks (approximately 5% of the cores cracked) and did not break when handled. The nonpigmented final product produced usable cores and acceptable final castings.

2.1.1.2 Resin Development Problems

The polyester resin selected during the early development efforts was a commercially available resin for commonly used casting imbedded samples. The early tests involved small samples with core elements imbedded in polyester. This resin flowed easily, cured slowly, and the early casting development was accomplished. However, when the complex fragment structure was cast, this resins shrinkage was sufficient to crack the samples. Attempts were made to reduce the cracking by using a minimum amount of catalyst to achieve a cure with a minimum temperature rise due to the exothermic curing reaction. The cure temperature was reduced to below 130°F and still the casting cracked. The commercial sources were searched and a low shrinkage "mass casting" resin was obtained and combinations of resin and catalyst were evaluated until the "mass casting" resin with its minimum recommended catalyst was found to produce usable castings. This was an unfortunate problem in that it resulted in scraping a large number of cores in cracked test specimens.

2.1.2 Liquid Flow Studies

Based upon the heat sink structural concept[*] it was expected that the structure and fragments could be cast using investment casting techniques. The flow studies involved experimentally evaluating the cavities or discontinuities which could hold bubbles during casting. The core development evolved from (1) to (4) in Figure 2.1. The cavities within and between the cores and the assembly results in possible flow and filling discontinuities.

The flow studies were carried out in flat plate acrylic molds. A core structure was assembled, a rectangular flat plate mold was fabricated and flow through and around the cores was evaluated. The angular variation allowed was checked using water as a surrogate. The final check and the experimental evaluation of flow and shrinkage used the polyester resin.

[*] I. B. Osofsky and L. E. Dunbar, "Light Weight Heat Sink Concept Development Study-Final Report", AMMRC-TR-81-42, August 1981.

5

The production of the integrated multilayer fragmenting steel concept will involve cores which are assembled using core tape of the type shown in Figure 2.2. If the application requires the warhead to be small (approximately 15 cm (6 in)) the ceramic cores will be fabricated as large segments including many fragment cavities. The individual cores used in this development may or may not be in intimate contact at the core edges, as a result of being assembled in the form of a cylinder or cone. To study a controlled case it was decided to consider the worst case for the flow studies with the minimum interconnections between cavities. The surrogate wax cores were joined together along their edges and sealed with a "sticky wax". This limited the flow to the geometric flow paths exposed to the skins of the fragment samples.

It was noted that if all the core interfaces and intersections of a perfect core structure were sealed with sticky wax, the two surface layers of fragments were not connected through the composite thickness. This is seen when observing the geometric configuration of core assembled and sealed on their edges. The wax core structure was a continuous layer of wax which would separate the two fragment layers. It was necessary to drill holes at the apex of the tetrahedra to form the truss connection between the two fragment layers and through the structure. This sealed core configuration provided some geometric insight into the structure which can be discussed as a three dimensional truss structure with the joints formed at the four tips of each tetrahedra.
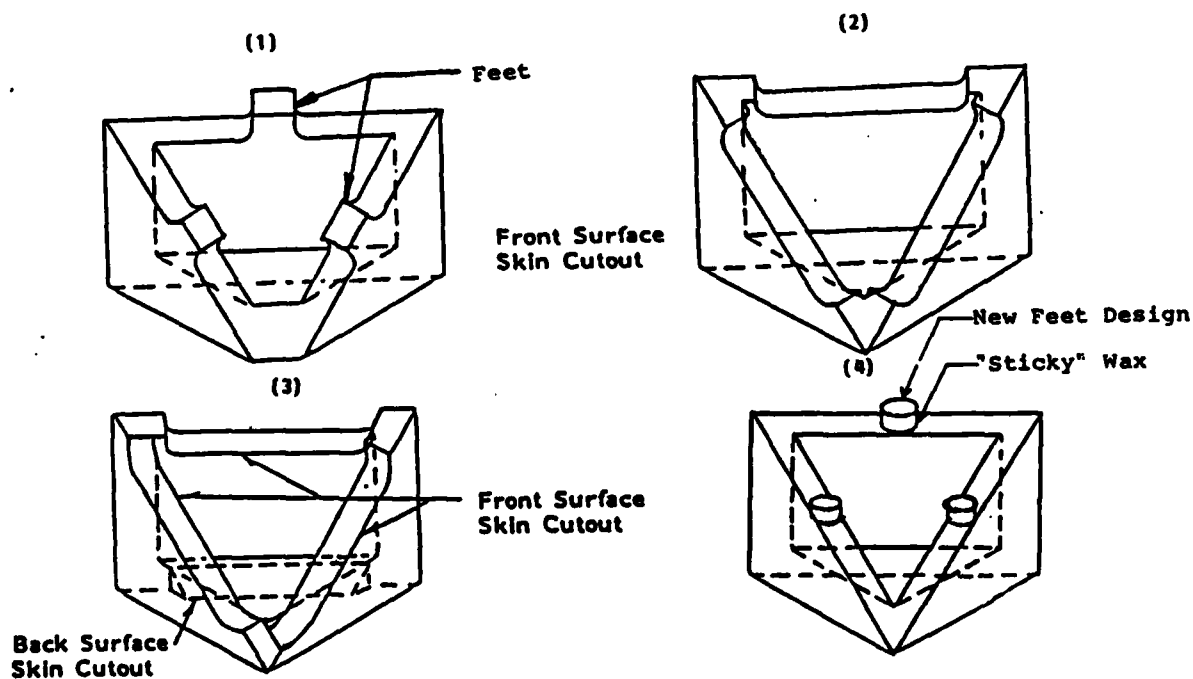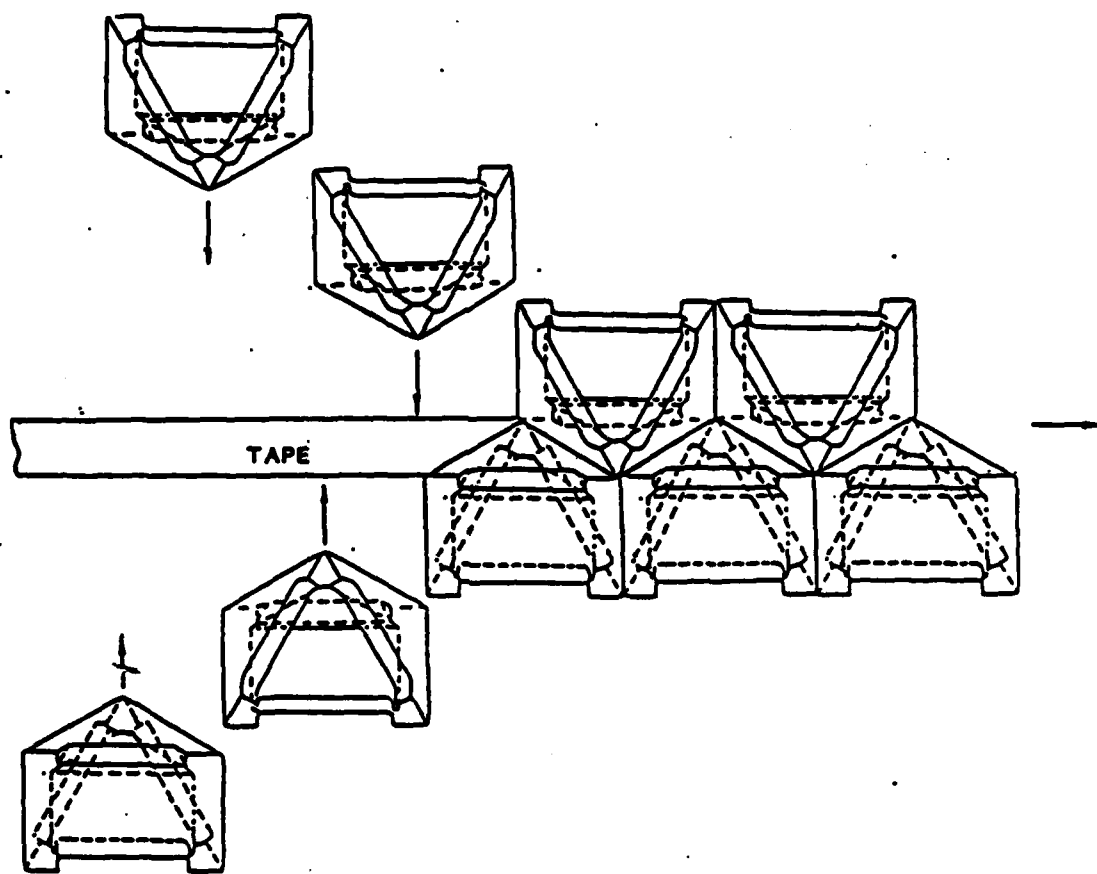
Figure 2.1 CORE DEVELOPMENT (1) to (4)

Figure 2.2 CORE TAPE CONFIGURATION

2.1.3 Casting Limitations

The casting limitations were found to be limited by the core geometry at the mid plane of the half octahedral fragments. Bubbles could be trapped in the octahedral core. If the structure is rotated with respect to gravity, such that the triangular sides of the half octahedral fragment is horizontal it would trap air. It was also determined that if this were the case the core could be designed with holes in the core wall to allow the trapped air to escape. The rectangular base of the half octahedra (see Figure 2.3), however, fits against a matching base on its mirror image. The geometry constrains this to +/-19.4° as shown in Figure 2.3. The X-axis is along the edge of the triangular opening surface intersecting the rectrangular base of a half octahedra. The X-axis is also designated as 0° direction later on. The Z-axis is perpendicular to the X-axis and both axes are on the plane of the triangular opening surface. If this must be violated, the base can be designed with a full width slot to allow the trapped gas to flow from one cavity to another. The concept used in this study is constrained in its casting angle of rotation, however, design modifications could easily be made in the core design to eliminate these constraints.

The casting limitations of the simple geometry are the result of flat surfaces within the ceramic core. If the design is such that these gas trapping situations could not be prevented, the core can be modified with holes to allow trapped gasses to escape.
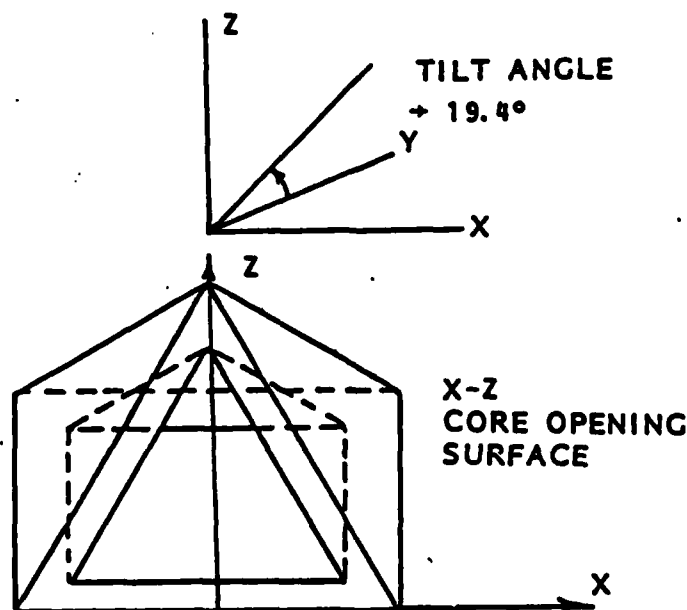
Figure 2.3 TRAPPED AIR CONSTRAINTS IN HALF OCTAHEDRA

## 2.2 Flat Plate Design and Development Tests

2.2.1 Flat Plate Design

The flat plate design was evolutionary. The plate design changed as the core design evolved. The original core tooling shown in Figure 2.1-(1) would produce 20 gm fragments if the "feet" or core supports were cut from the core walls. However, when it was decided to add wax "feet" (See Figure 2.1-(4)) to the core, the fragment size increased. The final result was a 45 gm (steel equivalent) fragment with a 0.152 cm (0.060 in) skin and a 40 gm (steel equivalent) fragment with a 0.076 cm (0.030in) skin. The fragment mass for various core dimensions is found in Appendix A.

2.2.2 Bending Test Design

It was intended that the bending tests be carried out in the two major directions in the fragment construction. These are the 0° and 90° directions shown in the lower left corner of Figure 2.4. This Figure is a reproduction of the surface of a cast test sample with the orientations superimposed. This can also be seen as the X and Z directions in Figure 2.3. The 0° and 90° properties can be resolved into the properties in any direction.

It should also be noted in Figure 2.5 that in the normal or production case a row of cores may shift relative to the next row of cores. This core shift or glide plane for assembly freedom will be used in fabricating cylinders or cones where each row of cores must shift with respect to its neighbor either to make up for the diameter change along the cone or the radial change around the cylinder. For simplicity and understanding the cores were assembled with coordination between the tips in the perpendicular (90° or perpendicular to base of surface triangle) direction.

The cast surrogate plates have a unit cell (edge length of the tetrahedra) dimension of approximately 2.8 cm (1.1 in) and the test fixture was designed to produce 4 point bending with the constant bending region covering approximately 2 unit cells. This will provide constant bending region at each of the sections of the unit cell and correct for any edge effects from the test fixture.

TOP SURFACE CONNECTIONS

GLIDE PLANES

CORE SUPPORT FEET

BOTTOM SURFACE CONNECTIONS

90°

0°
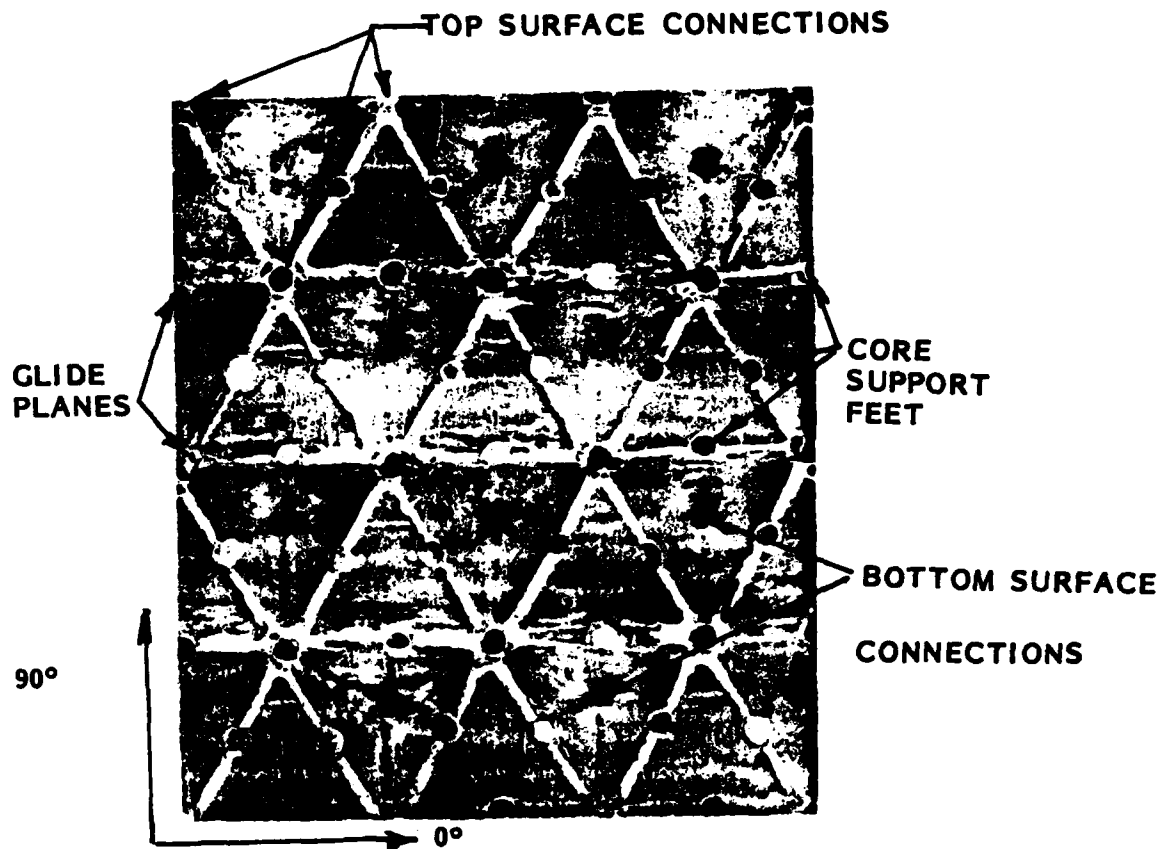
REPRODUCTION THROUGH POLYESTER

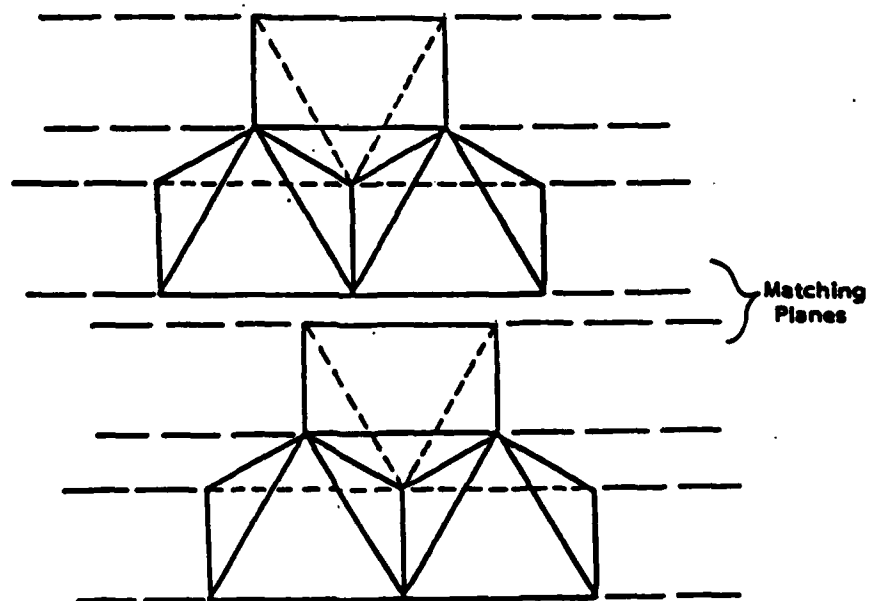Figure 2.4 CORE SURFACE GEOMETRY

Matching Planes

Figure 2.5 CORE SHIFT OR GLIDE PLANE
(THE PLANE OF THE RECTANGULAR BASE)
(USEFUL FOR ASSEMBLY FREEDOM)

10

Figure 2-6 is a schematic of the test fixture designed for these tests. The tests were accomplished by using either a 15.24 cm (6 in) or 20.32 cm (8 in) span between supports of the four point loading fixture. In this way, the testing was accomplished at one span, adding the dead loading and measuring the deformation across the range of loads. Then repeating the same range of load with the second span to produce two different moments for the same load. The surrogate polyester specimen had deformed slightly during wax melting and removal. The specimens had a small twist which was deformed to flat by the initial loadings. This twist did result in a low load nonlinearity in the deformation history.
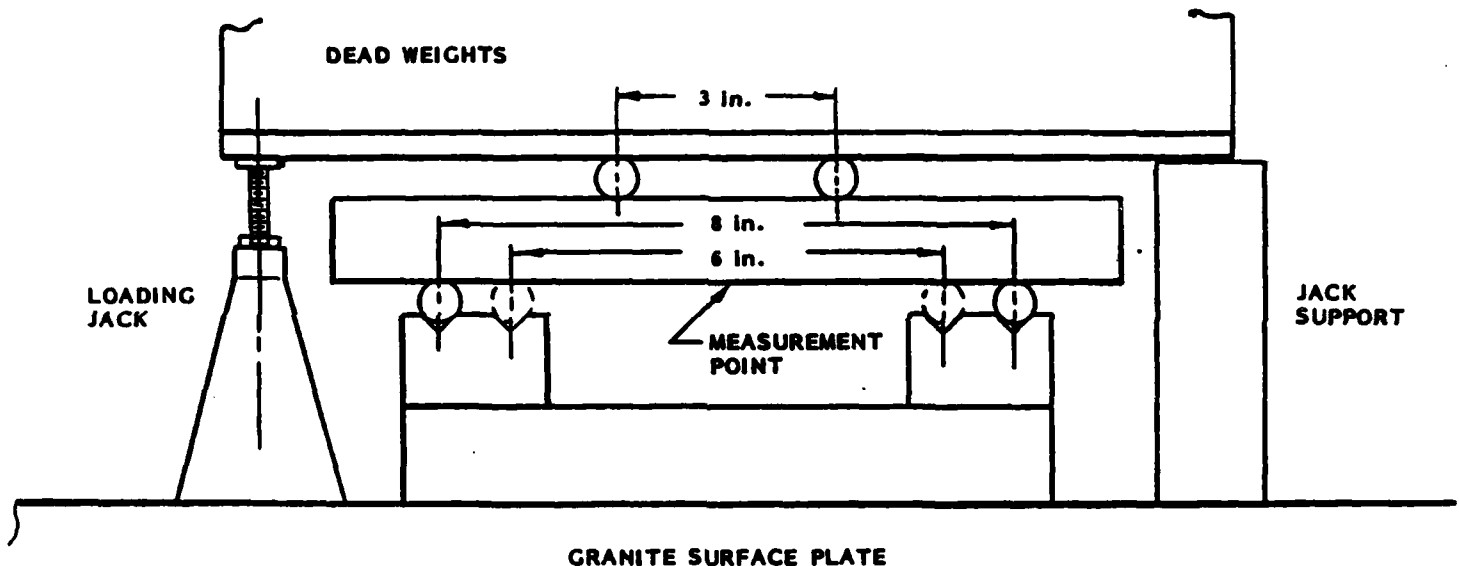
Figure 2.6 FOUR POINT BENDING FIXTURE

The testing was accomplished by measuring the deformations with respect to the granite surface plate for each load level. The deformation load history was measured during unloading to eliminate the effects of any plastic deformations which might occur at the load points during the increasing loads. It did not correct for the elastic changes which were checked by measuring the position of the loading rods at each dead load. The testing was carried out in the elastic range of the test samples. Sufficient data was obtained by testing below 72 kg (160 lb).

11

The total weight of 72 kg (160 lb) made up of increments of 14 kg (30 lb) dead weight was applied gradually to the specimen using a screw jack. The deformation of the specimen was measured using dial indicators referenced to the surface plate. Measurements were taken on both sides of the beam in order to determine when the original twist deformation dominated the readings.

The 14 kg (30 lb) dead weights were incrementally removed and the change in deformation measured. This data remained in the linear range down to approximately 35 kg (77 lb) where twisting effects from the original preset distorted the results (See Appendix II).

2.2.3 Bending Test Results

The tests allowed a comparison of the multilayer fragment composite to an equivalent solid beam in a similar test configuration. This provides a basis for comparing this structural concept to an equivalent monocoque or solid skin composite construction. The comparison involved measuring the surrogate material's modulus and load deformation history. These data allowed a prediction of the equivalent solid thickness for the same deformation history.

Solid cast polyester beam samples of the type shown in Figure 2.4 were used to measure the as cast surrogate material modulus. Using the measured geometry the moment of inertia was calculated. Using this and the load displacement history allowed the modulus to be calculated. The modulus for this polyester "mass casting" resin was 7.84×10^3 MPa (1.12×10^6 psi).

The composite multilayer fragmenting beams were tested in bending. The data was collected and preliminary plots (See Appendix II) showed a sharp break in the linear range. This was caused by an initial twist in the sample. The first slope occured as the beam straightened. The data above this break was reduced using a least squares fit to describe the deflection history. The results of the data reduction are shown in Table 2.1.

These tests have shown an integrated composite approximately 2.8 cm (1.1 in) thick with a nominal 1.5 mm (0.060 in) skin is equivalent to a 1.5 cm (0.6 in) solid plate in four-point bending. This suggests that the concept of integrated construction will be very beneficial for both cost and weight saving in an interceptor design.

12

2.3 Surrogate Program Results

The data in Table 2.1 justified proceeding to develop the multilayered fragmenting warhead structure concept in steel to determine the concepts properties for a nonnuclear kill warhead. The scatter in the limited data and the nonuniformity of the fragment construction do not allow a "micromechanical" prediction of the composite mechanical properties, except to suggest that its stiffness is approximately that of a solid of the same solid mass (The fragment construction is 60-75% solid.).

Table 2.1 TEST RESULTS SUMMARY/SURROGATE BENDING TESTS
(2.8 CM THICK SAMPLES)

SAMPLE SKIN CM (IN)	TEST ORIENT-ATION	SLOPE (LEAST SQUARES) CM/N(IN/LB)	MODULUS* MPA(PSI)	EQUI.SOLID** MOMENT OF INERTIA CM^4(IN^4)	EQUIVALENT SOLID*** CM(IN)
SOLID RESIN	N/A	6.8×10^{-5} (1.2×10^{-4})	7.84×10^3 (1.12×10^6)	5.16 (.124)	2.54 (1.0)
0.152 (0.060)	90°	4.2×10^{-5} (7.4×10^{-5})	7.84×10^3 (1.12×10^6)	3.12 (0.075)	1.63 (0.64)
0.152 (0.060)	0°	11.4×10^{-5} (2.0×10^{-4})	7.84×10^3 (1.12×10^6)	1.17 (0.028)	1.34 (0.49)
0.076 (0.030)	0°	8.34×10^{-5} (1.46×10^{-4})	7.84×10^3 (1.12×10^6)	1.57 (0.038)	1.5 (0.59)

*CALCULATED FROM BEAM GEOMETRY
** MOMENT OF INERTIA CALCULATED AS THOUGH BEAMS WERE SOLID
***NORMALIZED TO UNIT WIDTH

3.0 PROTOTYPE CASTING TASKS

The technology developed in the surrogate efforts was converted to casting 17-4PH test specimens and characterizing these composite structures. It was anticipated that problems would occur in the transition from polyester/wax to steel/ceramic. Figure 3.1 shows a flow diagram for the casting of the samples. The fabrication of ceramic cores and their assembly into plates was expected to involve some changes in design from the wax surrogates. In addition, the positive or negative impact of the ceramic on the properties of the completed steel composite was an unknown to be answered.

ASSEMBLE CORES IN MOLD (SEE FIG. 3.5)
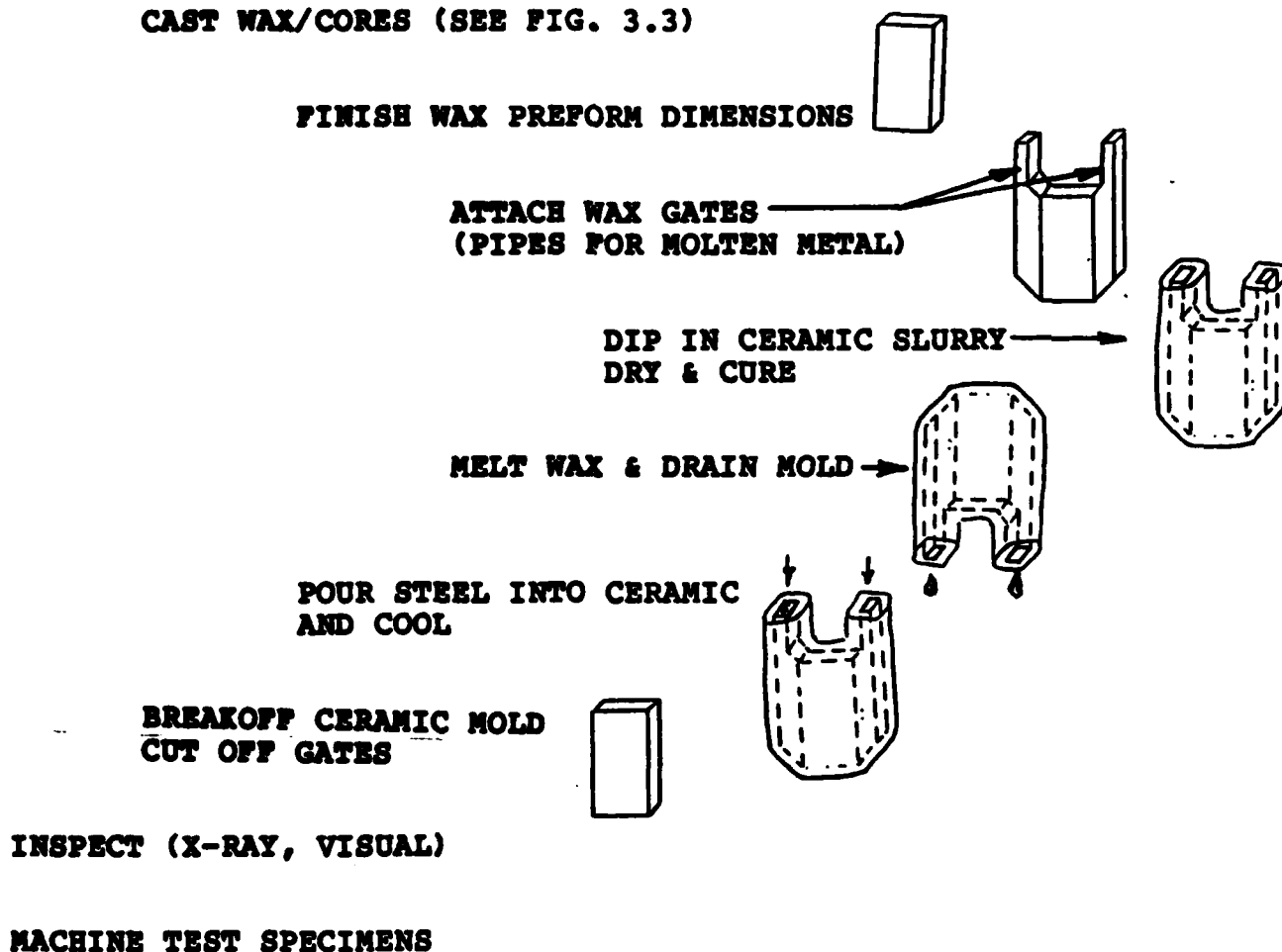
CAST WAX/CORES (SEE FIG. 3.3)

FINISH WAX PREFORM DIMENSIONS

ATTACH WAX GATES
(PIPES FOR MOLTEN METAL)

DIP IN CERAMIC SLURRY
DRY & CURE

MELT WAX & DRAIN MOLD

POUR STEEL INTO CERAMIC
AND COOL

BREAKOFF CERAMIC MOLD
CUT OFF GATES

INSPECT (X-RAY, VISUAL)

MACHINE TEST SPECIMENS

Figure 3.1 TEST SAMPLE FABRICATION FLOW CHART

14

3.1 Tooling Development and Core Fabrication

This activity involved conceiving a core concept and communicating this spacial concept to ceramic core die designer.

3.1.1 Core Design

The ceramic core concept was modified from that shown in Figure 2.1, where the stand-off feet were added to a concept by attaching then with sticky wax, to the ceramic core in which these feet were integral to the core and acted as push out plugs for the tooling. In the final tooling concept shown in Figure 3.2 the bottom of the core die consisted of a fixed plug shaped like a half tetrahedron with the parting or separation plane the same as the surface under the skin of the composite (See Figure 3.2 lower right). The feet were formed in small holes in the bottom half of the die. The plug fit into the core in the opening shown in the lower left section of Figure 3.2. The remainder of the core surface was formed in the female top of the die. The die was close, the ceramic slurry injected, allowed to set up, and the female portion of the die withdrawn exposing the outer surface of the half octahedral core. The plugs in the end of the feet hole then were used to push the core off the plug (See lower right section of Figure 3.2). The diameter of the feet was selected as small as possible to minimize the effect on the skin while still providing sufficient strength to act as a tooling "push out" used to remove the core from its internal die plug.

3.1.2 Core Fabrication

The prototype tooling was fabricated as a single cavity die. In production the cores would be made in a multiple cavity die. The complexity of the core shape cavity was put into the die using Electrical Discharge Machining (EDM).

3.2 Casting Development

The complexity of the concept with its multiple channels for metal flow and cavities to fill had suggested the need for vacuum casting to achieve soundness in the test specimens. Vacuum casting produces no gas formed cavities and achieves slower cooling and more likelyhood of sound casting. However, it is more costly and is limited as the size casting that can be made at one time. The requirement for vacuum casting was checked by first attempting to cast a specimen using air melt 17-4 PH.
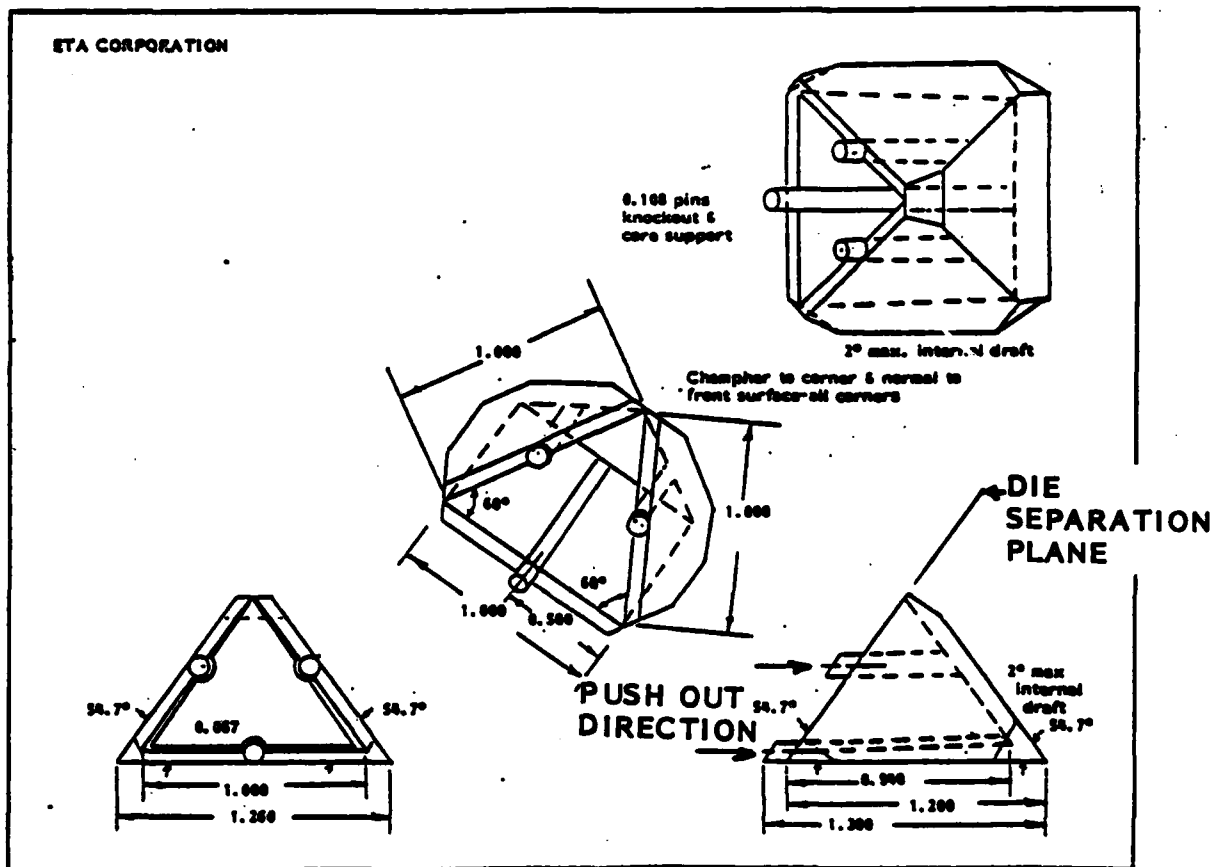
15

Figure 3.2 TOOLING CORE DESIGN

The tooling concept developed consists of acrylic sheets cut and grooved to assemble into a 9 in. long rectangular mold. The sides assemble into grooves in the top and bottom. The cores were assembled in these acrylic molds as shown in Figure 3.5 a - c. Following discussions with the investment casting specialists, this approach was approved and it was agreed to attempt the first casting using a soft clear wax (the same wax used in blending for the prototype development 2.1.1.) for the wax assembly.

Wax assemblies of the type shown in Fig. 3.1 (Step 3) above were fabricated. Numerous problems were encountered. The wax shrinkage during solidification and cooling is quite large and resulted in very wavy erratic surface. The problems were eventually solved by manually sculpturing the wax core assemblies.
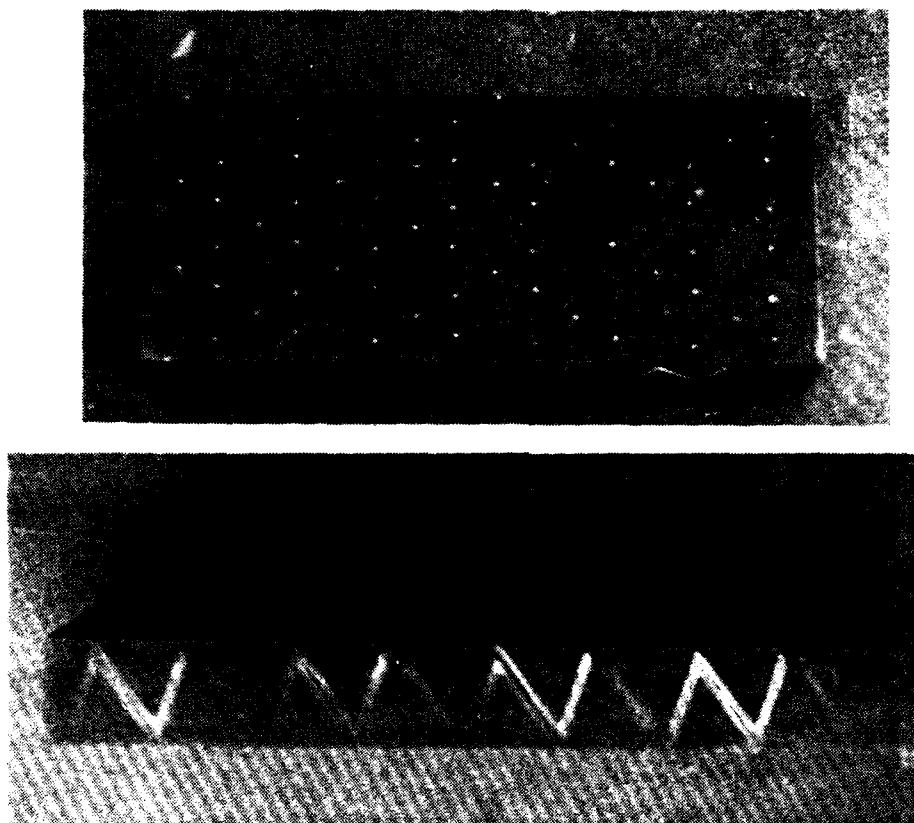
16

Figure 3.3 WAX MOLDING CONCEPT

Three wax forms were submitted to the foundry. The foundry experts discussed approaches to gating the casting and agreed to attempt a trial casting using one of the three wax forms.

The first trial casting was completed and is shown in Figure 3.4. The foundry was concerned about the shrinkage in the fragment cavities and had connected small wax gat̪s (tubes for molten metal) to each of the cav⁴ties on one side of the specimen. These gates were cut from the specimens leaving the appearance of small buttons on the surface as shown in Figure 3.4(a). This compares to the clear side Figure 3.4(b). An x-ray of the casting shows some minor shrinkage, however, the surface appears sound.

With this partial success, it was decided to attempt to cast using a clear surface and to switch to a harder commercial wax. The wax was ordered, obtained, and specimen assembly commenced. Figure 3.5 shows the core arrangement for a flat plate tensile and compression specimens for both the perpendicular and parallel orientation. The bending specimens are similar except the total specimen is filled with cores in order to eliminate any discontinuity in the specimen inside the outer loading points in the four point bending set up.

17

GROUND OFF GATE

(a)

(b)

Figure 3.4 FIRST CASTING

Since only a small number of samples (approximately 15) were to be cast, purchasing production wax injection tooling was not justified. It was decided to cast the forms using gravity rather than pressure to achieve soundness in the cast wax. The program suffered by encountering numerous injection (casting in this case) problems. The assembly of wax forms was much more difficult and time consuming than planned. The shrinkage problem encountered earlier with the wax shrinkage inside the ceramic core was approached by filling the half octahedral cores with wax and then assembling these partially filled cores in the mold. Then pouring molten wax in the tetrahedral cavities to complete filling the cavities. This reduced the amount of molten wax in the final pour and thus the shrinkage. Figure 3.6 shows a specimen layout in which the cores have been filled with wax. The shrinkage holes can be seen in the middle of the wax. The shrinkage and casting problems were solved by manually sculpturing the wax specimens.
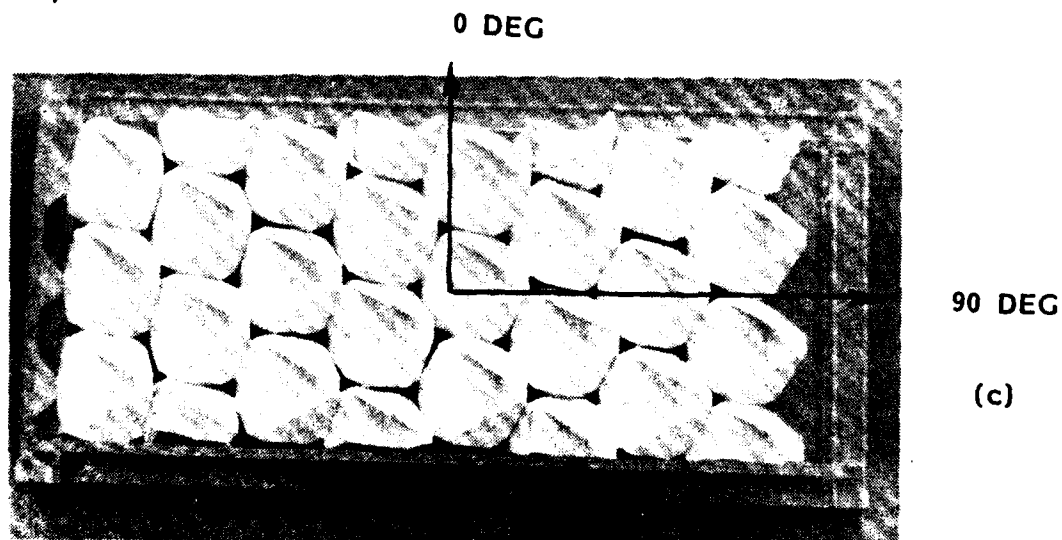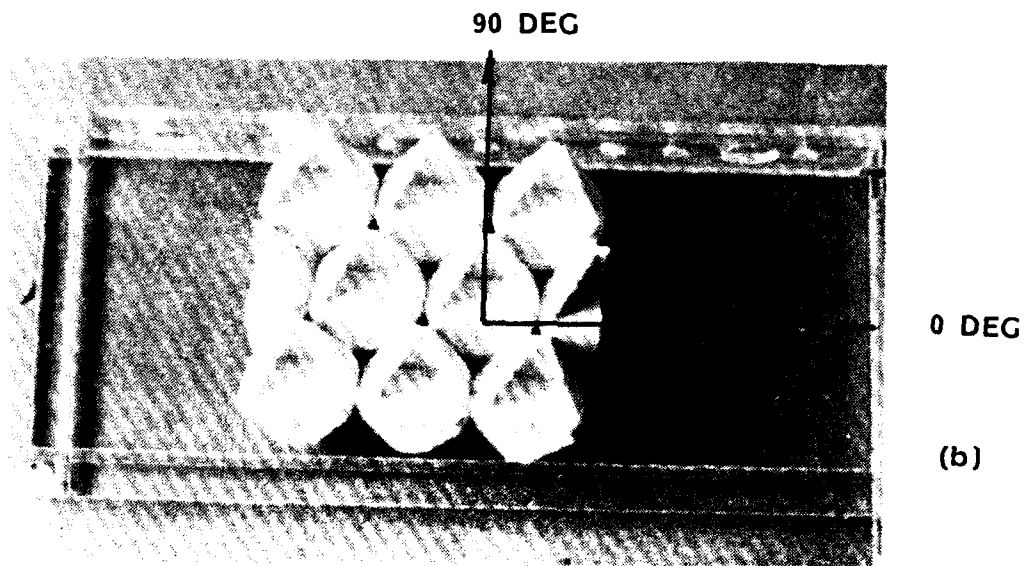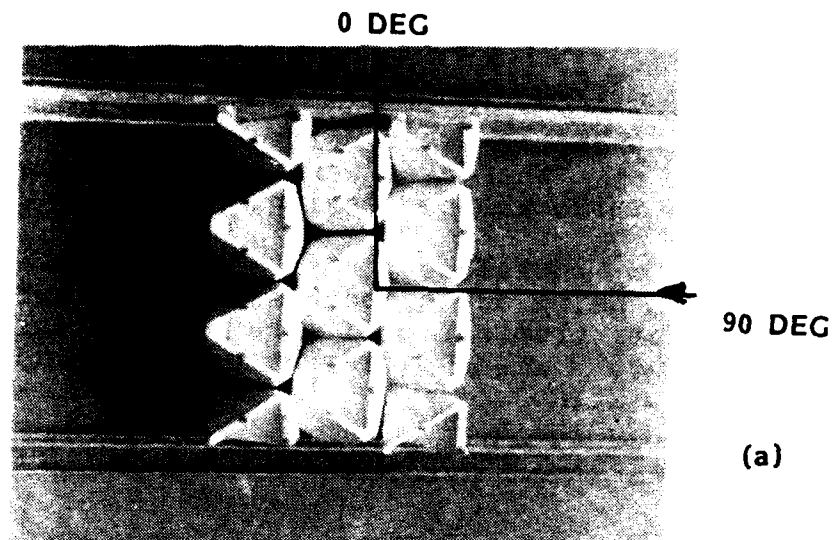
0 DEG

90 DEG

(a)

90 DEG

0 DEG

(b)

0 DEG

90 DEG

(c)

Figure 3.5 CORE ARRANGEMENT FOR SPECIMENS

19

The wax preforms were delivered to the foundry for gating and casting. The gates were varied during set up in an attempt to optimize the processing.

Gates were installed as single and multiple strips along the specimens on one or both sides. The gates in some cases were wider than one cell size and the cores were no longer constrained. These different orientations are shown in Figures 3.7 to 3.10.
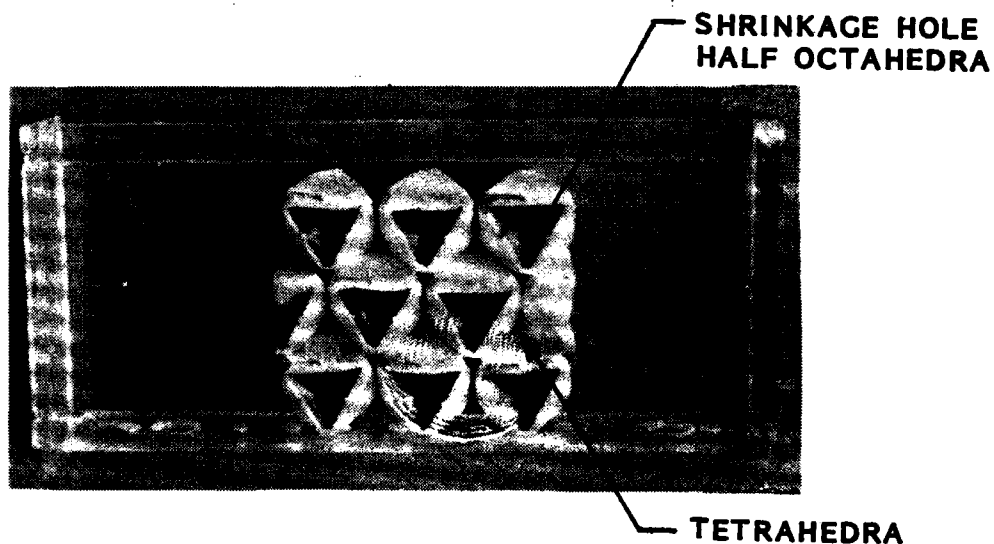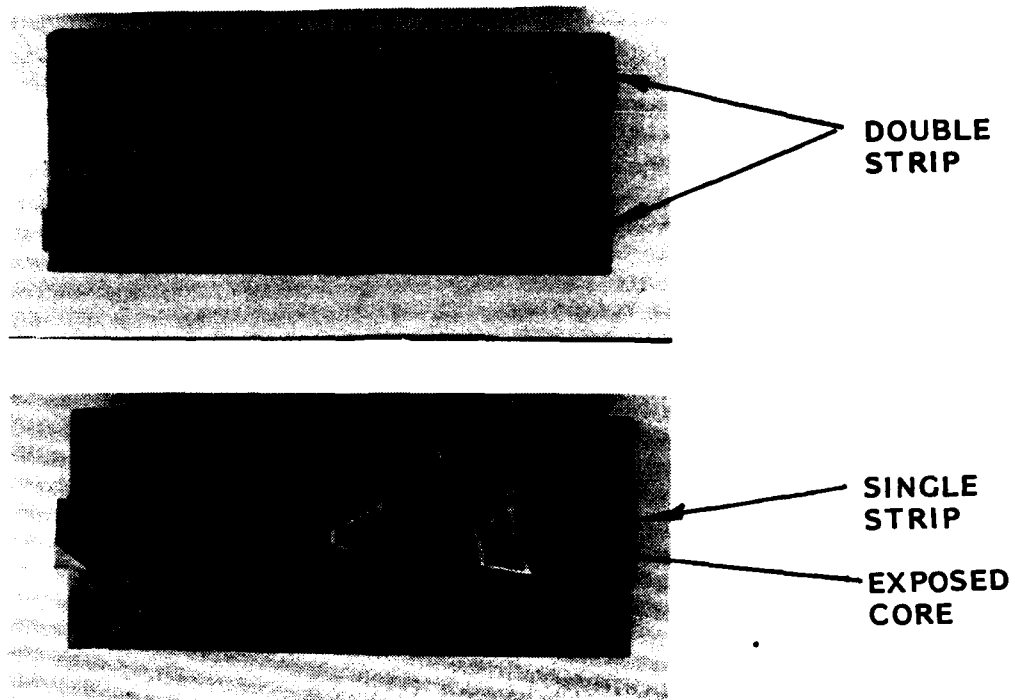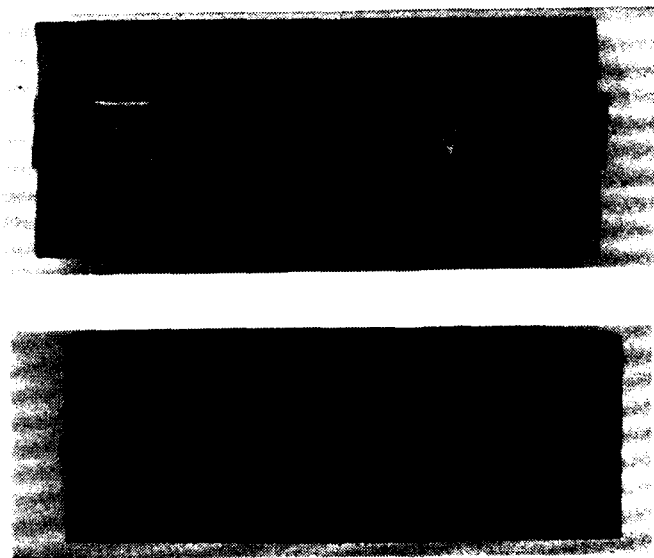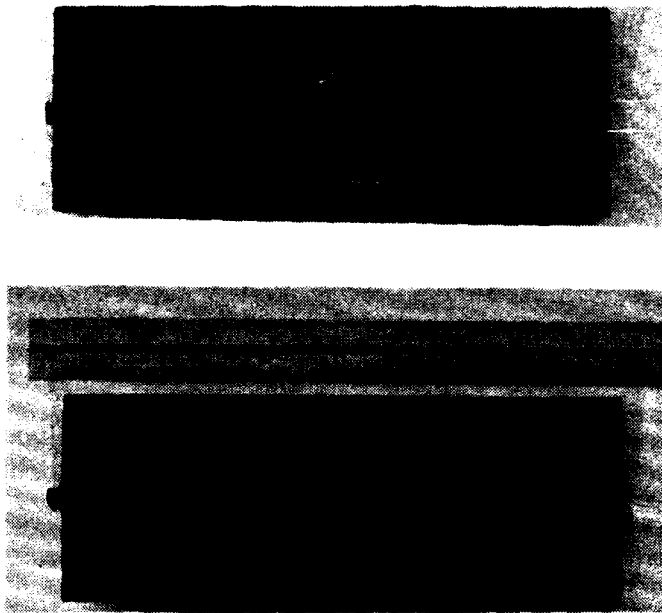

Figure 3.6 WAX SHRINKAGE IN CORES

DOUBLE
STRIP

SINGLE
STRIP

EXPOSED
CORE

Figure 3.7 DOUBLE/SINGLE STRIP GATING

Figure 3.8 WIDE SINGLE STRIP GATE/CLEAR (NO GATE)

21

Figure 3.9 DOUBLE/CLEAR GATING

Figure 3.10 EDGE GATED CASTINGS
INSUFFICIENT MOLD STRENGTH - SIDES FAILED.

22

The castings were x-rayed and the x-ray plates were inspected and an orientation was established with respect to the casting in question. These plates provided the first evaluation tool. Then the castings were inspected to find flat surfaces from the original preform that could be used as reference for grinding. The grinding was accomplished by magnetically holding the samples on the existing flat areas and grinding the gates from the opposite side, then flipping sides, magnetically holding the samples and grinding the other. The grinding operation was monitored continuously, inspecting the surfaces to determine the variations from a flat surface. During the grinding it was observed that the test areas (those area containing cores) were flat to within 0.025 cm (0.010 in). A large amount of shrinkage was observed in the noncored areas. However, this was not essential to test specimen operation. Also the movement of the unconstrained cores was observed when these cores were exposed by grinding off the gating. The finished specimens showed flat ground areas, unground areas resulting from shrinkage, and exposed cores that had moved into the gating during the casting.

To aid in laying out areas for acceptable test specimens the ground specimens were set on a copying machine to produce a paper record of the surface. An example of this record of surface non-uniformities as shown in Figure 3.11. Sample 15 shows a shrinkage hole in the right end of the front. The x-ray showed this hole joined internal porosity in that end. The back and front of the Sample 15 show the surface to be acceptably flat even into the grip ends. Sample 10 is an example of shrinkage in the solid ends of the casting. In this case the x-ray plate showed the ends to be sound. The shrinkage on both samples was acceptable for the friction grips of the tensile specimens and using a dog bone configuration made this shrinkage outside of the gage length acceptable for compression specimens.

Comparing the surface copies with the x-ray plates allowed the selection of relatively flaw free areas for cutting specimens. The test specimen areas were chosen such that the gage length contained essentially flaw free core structure. Defects were allowed outside the gage length and in the grip areas. The tensile and compression specimens were modified dog bone shaped as shown in Figure 3.12. Each specimen was designed to test an acceptable area of the casting. The flexure specimens were long rectangular columns as shown in Figure 3.12. The specimen dimensions were variable and were chosen to provide sound composite material within the gage length. The minimum width was one cell size and the largest was two cell sizes wide.
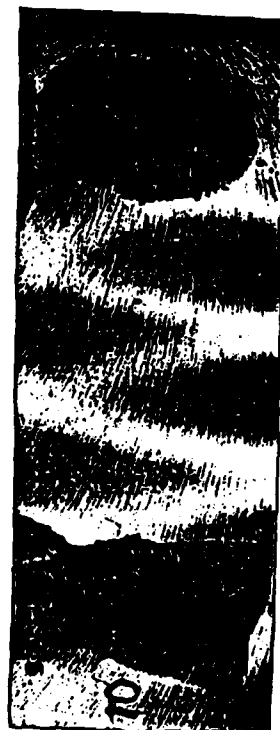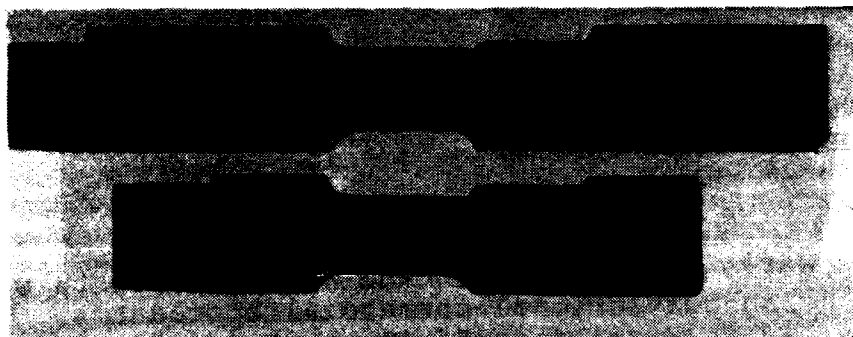
23

(Sample 15 front)
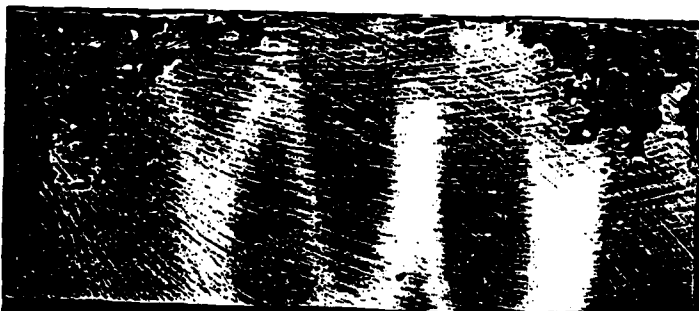
(Sample 15 back)

(Sample 10)

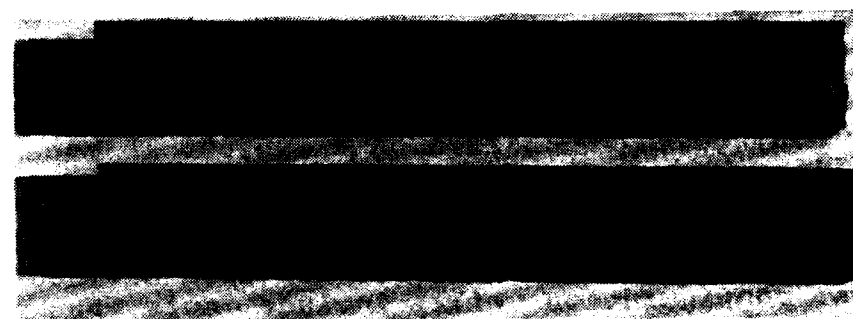Figure 3.11 REPRODUCTIONS OF CASTING GROUND SURFACE
(REDUCED FOR DISPLAY)

TENSILE
SPECIMEN
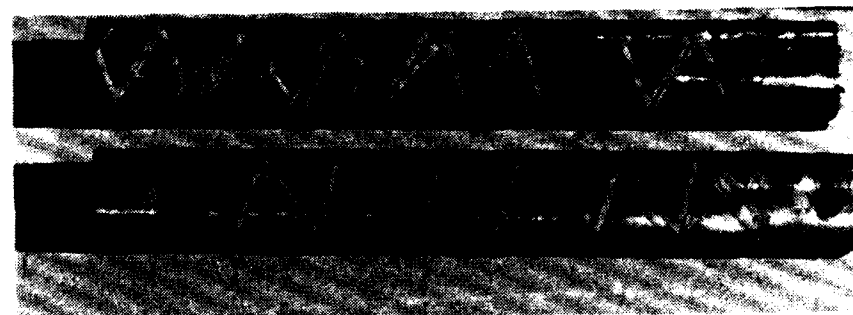
COMPRESSION
SPECIMEN

SIDE VIEW

FLEXURE
SPECIMENS

SIDE VIEW

Figure 3.12 SAMPLE TEST SPECIMENS

4.0 FLAT PLATE CHARACTERIZATION

4.1 Test Procedures

The tensile, compression, and flexure tests were carried out using conventional commercial approaches. The tensile tests were carried out in a hydraulic tensile machine with a 60,000 lb capacity. The modified dog bone tensile specimens were loaded through friction grips and the modulus was measured using a clamp on strain gage extensometer. Figure 4.1 is a typical reduction of a loading trace for a tensile test. The compression tests were carried out at the low levels in the same machine except the loading was done on the parallel ends of the specimens. The brake in the trace in Figure 4.1 occurred when the extensometer is removed to avoid damage to it. In both the tensile and compression case the extensometer was removed after sufficient data to find a modulus. Figure 4.2 is a typical reduction of a trace of a compression test of a specimen taken to failure. It was learned that the 0 deg orientation (0 deg means the glide plane coincides with the load direction--See Figure 2.4) compression specimens were slightly stronger than the 90 deg orientation specimens. These specimens were removed after the modulus was measured and taken to failure on a 120,000 lb machine at another facility.

The flexure tests were accomplished using a 4-point bending fixture with a 20.19 cm (7.95 in) span divided in thirds. This configuration will include more than two cells and almost three cells in the inner third or constant bending region. The initial bending modulus was measured using a strain gage deflectometer. This was removed and the specimen taken to failure. Figure 4.3 is a reduction of the load deflection trace of a flexure test.
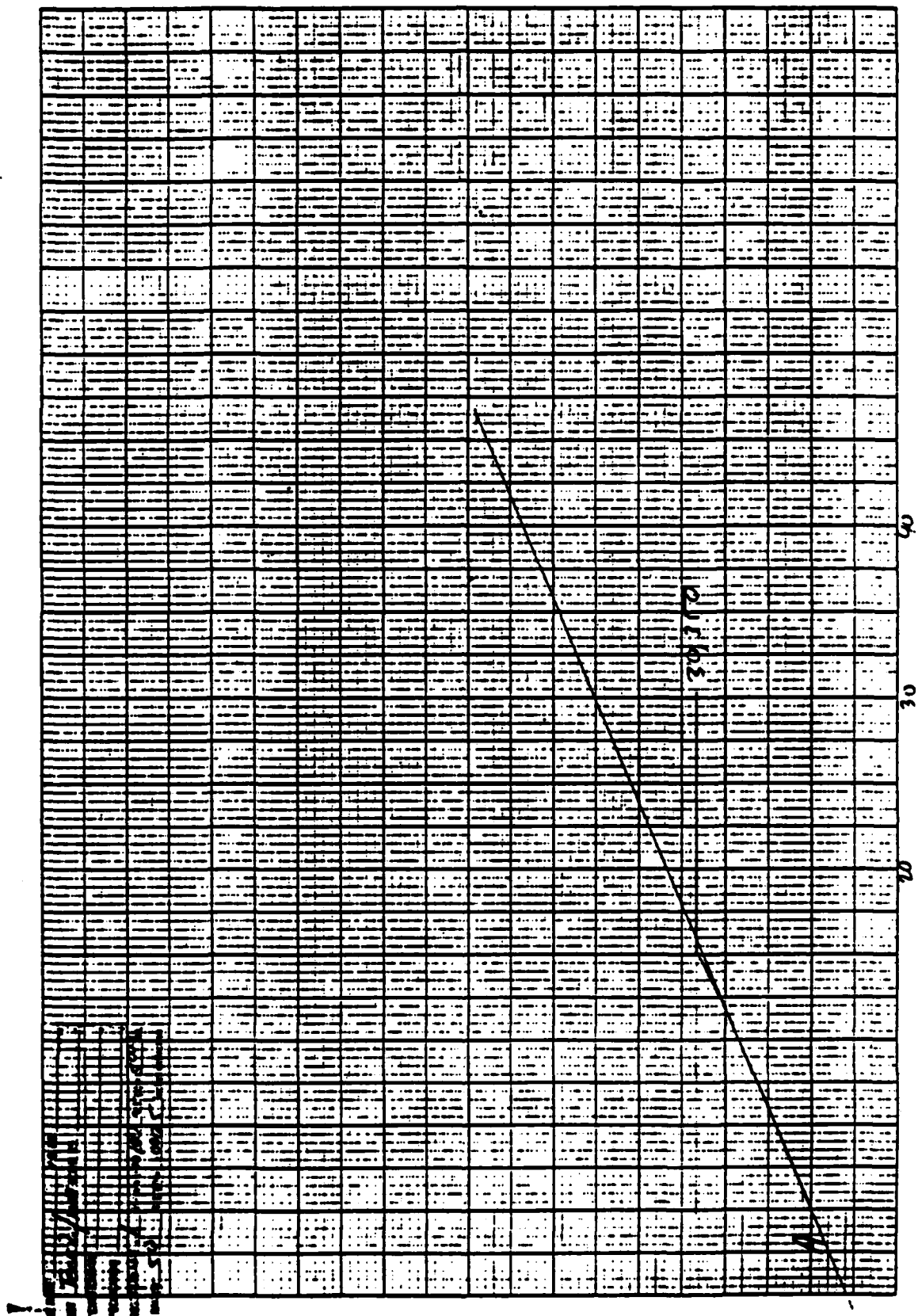
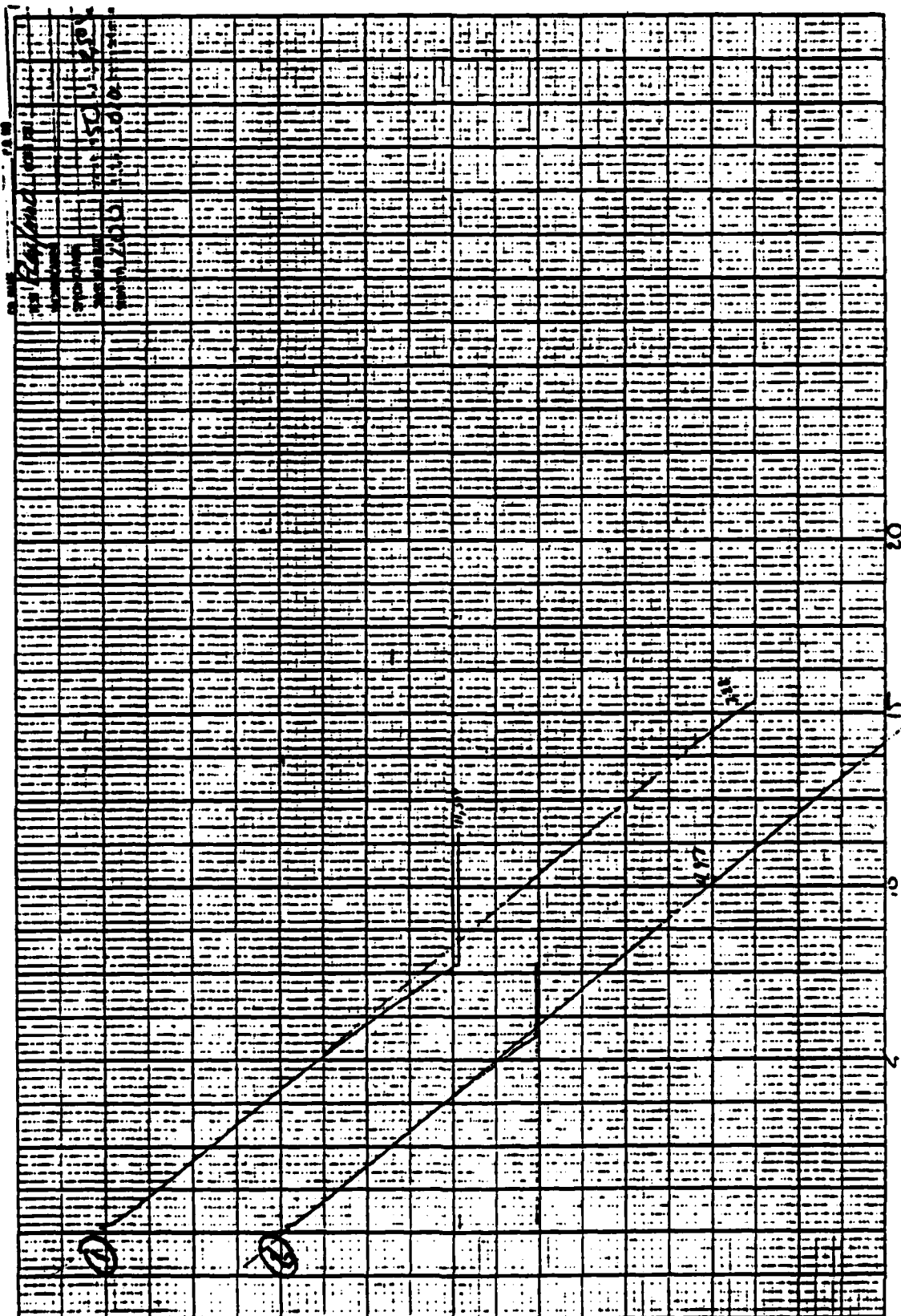Figure 4.1 LOAD DEFLECTION TRACE FOR A TENSILE TEST

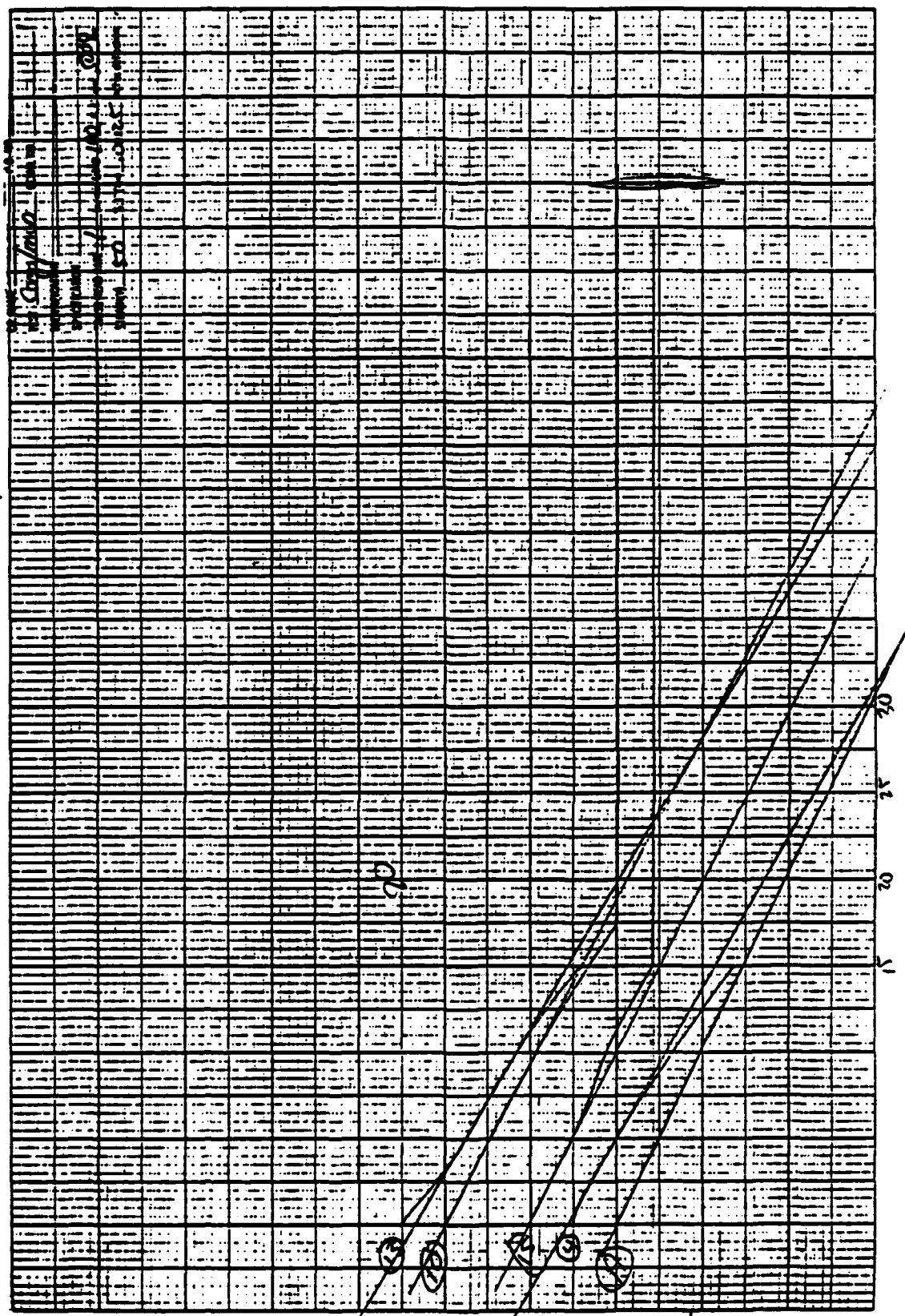Figure 4.2 LOAD DEFLECTION TRACE FOR COMPRESSION TEST

Figure 4.3 LOAD DEFLECTION TRACE FOR FLEXURE TEST

4.2 Test Results

The reduced data is presented in Tables 4.1 to 4.6. where the spread in the data was far less than expected. Observing the test specimens before the tests showed potential flaws and nonuniform core distributions resulting from the casting problems. During the tests the failure was observed to be concentrated in the skin areas between fragments with shear banding appearing on the surfaces across more than one area between fragments. This concentration of deformation and the ductility may explain the reduction in the expected scatter. Improved production processing should reduce the scatter.

Table 4.1 0 DEG ORIENTATION TENSILE TEST

CASTING NUMBER	WIDTH IN.	THICKNESS IN	MODULUS KSI	ULTIMATE LOAD KLB	ULTIMATE STRESS KSI
7	1.123	1.128	7.38	14.50	11.45 SURFACE FLAW
10	0.816	1.100	7.75	21.88	24.37
11	1.706	1.100	6.55	31.00	16.52
AVE.			7.23		17.45

Table 4.2 90 DEG. ORIENTATION TENSILE TEST

CASTING NUMBER	WIDTH IN.	THICKNESS IN	MODULUS KSI	ULTIMATE LOAD KLB.	ULTIMATE STRESS KSI
A	1.437	1.100	6.02	30.35	19.20
3	1.250	1.108	6.89	20.00	14.44
4	1.566	1.098	5.47	34.50	20.06
15	1.449	1.100	6.23	33.40	20.95
AVE.			6.15		18.67

Table 4.3   0 DEG ORIENTATION COMPRESSION TEST

CASTING NUMBER	WIDTH IN.	THICKNESS IN	MODULUS KSI	ULTIMATE LOAD KLB	ULTIMATE STRESS KSI
7	1.108	1.103	8.57	81.00	66.28
10	0.838	1.100	8.18	65.00	70.51
13	0.959	1.100	8.19	58.00	54.98
AVE.			8.31		63.92

Table 4.4   90 DEG ORIENTATION COMPRESSION TESTS

CASTING NUMBER	WIDTH IN.	THICKNESS IN	MODULUS KSI	ULTIMATE LOAD KLB	ULTIMATE STRESS KSI
A	1.155	1.100	6.42	87.00	68.48
3	1.108	1.103	5.82	57.50	47.05
4	1.080	1.100	6.41	61.00	51.35
15	1.012	1.100	7.15	57.38	51.55
AVE.			6.45		54.60

31

Table 4.5 0 DEG ORIENTATION FLEXURE TEST

CASTING NUMBER	WIDTH IN	THICKNESS IN	MODULUS KSI	ULTIMATE LOAD KLB	ULTIMATE STRESS KSI	EQUIV. THICK.
9	1.084	1.100	12.40	18.75	110.00	0.84
9	1.156	1.100	12.04	7.52	42.38	0.84
AVE			12.22		76.19	0.84

Table 4.6 90 DEG. ORIENTATION FLEXURE TEST

CASTING NUMBER	WIDTH IN	THICKNESS IN	MODULUS KSI	ULTIMATE LOAD KLB	ULTIMATE STRESS KSI	EQUIV. THICK.
1	1.209	1.100	12.26	11.55	60.76	0.73
6	1.258	1.100	11.50	7.75	39.18	0.82
14	1.147	1.087	8.99	12.75	70.15	0.76
AVE			10.92		56.70	0.77

Figures 4.4 to 4.7 show the before and after for tensile tests carried out on specimens with 90 deg orientations. Notice the surface deformations associated with the fragment structure inside the structure. Figures 4.8 to 4.10 show the before and after for compression specimens in the 90 deg orientation. The ceramic cores had a minimal impact on the tensile specimens, however, they became involved carrying load during the compression deformation. In Figure 4.4 note the extensive deformation which occurred in bands between the fragment specimens. Figure 4.10 shows a fragment almost torn free of the specimen.
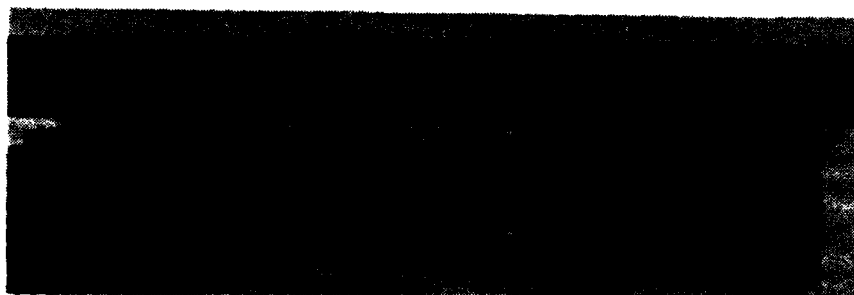

SHEAR BANDS
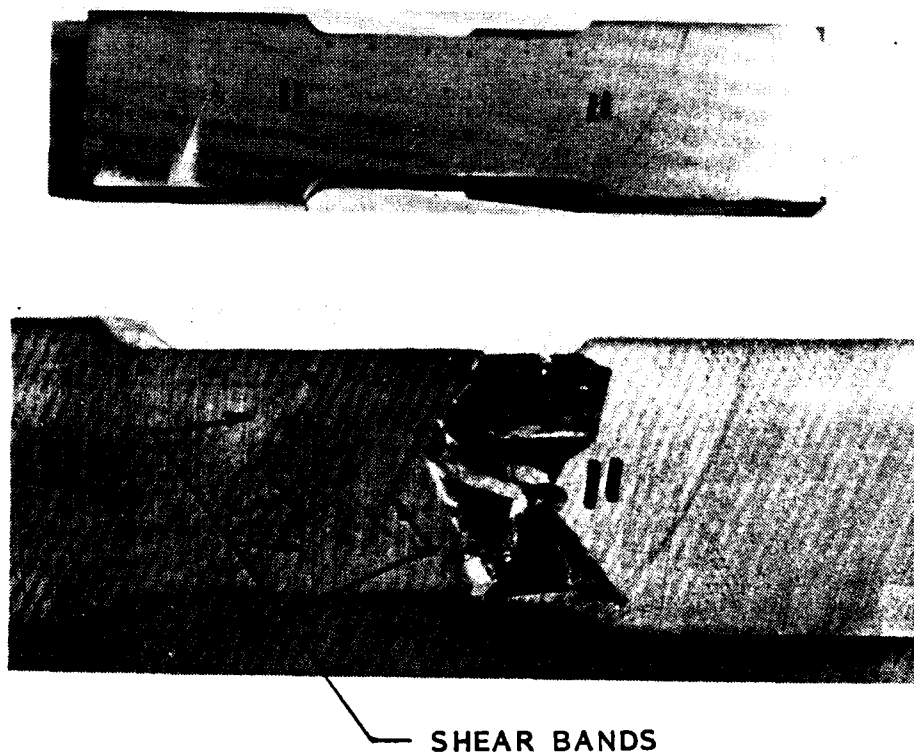
Figure 4.4 TENSILE TEST SPECIMEN NO. 11
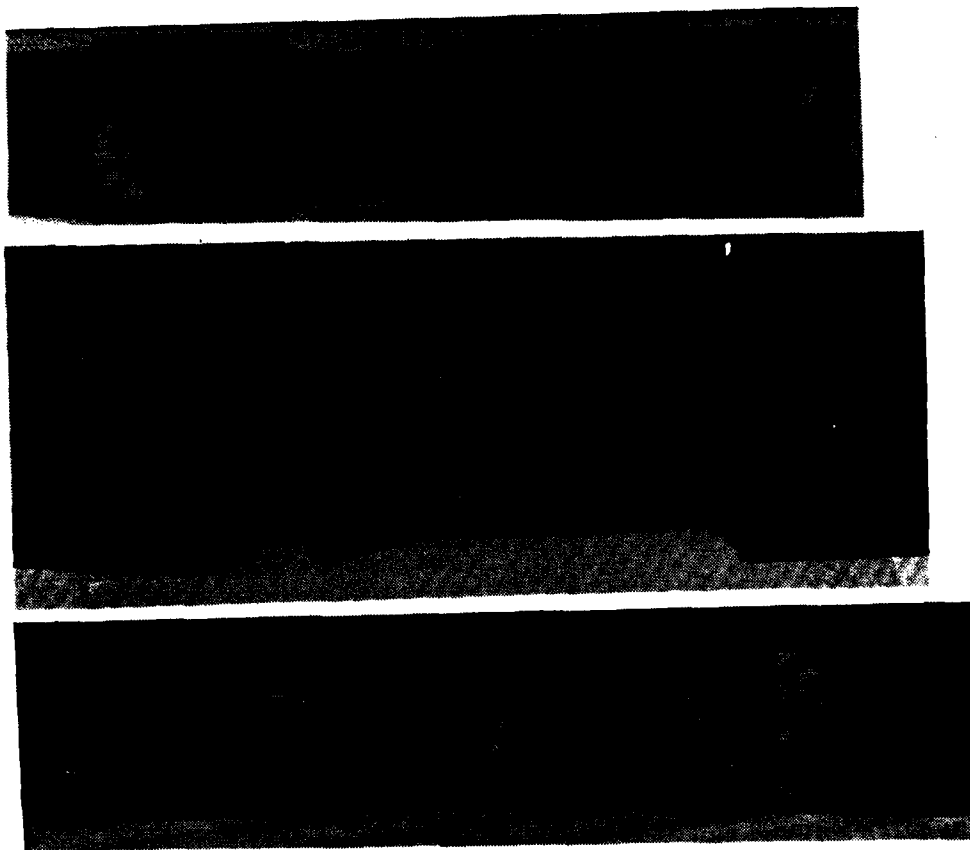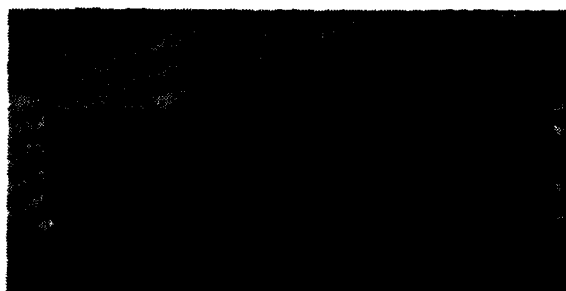
Figure 4.5 TENSILE TEST SPECIMEN NO. 4
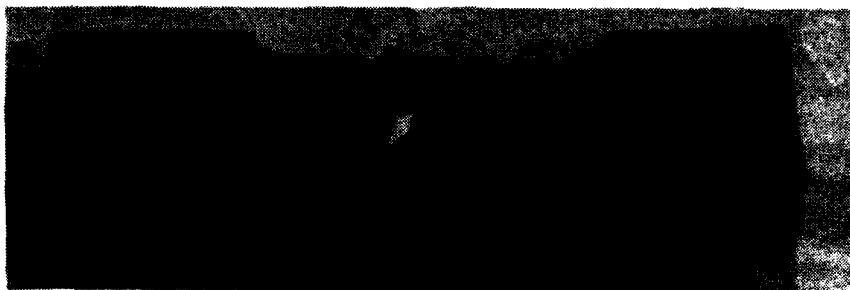

Figure 4.6 TENSILE TEST SPECIMEN NO. 15

34

Figure 4.7 TENSILE TEST SPECIMEN NO. 3


Figure 4.8 COMPRESSION TEST SPECIMEN NO. 3

Figure 4.9 COMPRESSION SPECIMEN NO. 10
ALONG 0 DEGREE DIRECTION

Figure 4.10 COMPRESSION TEST SPECIMEN NO. 7
ALONG 90 DEGREE DIRECTION

Figures 4.11 and 4.12 show the flexural failure for the 0 deg and the 90 deg orientations. In almost all cases the failure occurred at a casting flaw. This probably produced a lower strength than could be expected. However, since the moment of inertia for a solid beam (width x thickness^3/12) as a first approximation is the cube of the thickness, the flaws had a lesser affect on the elastic measurements.
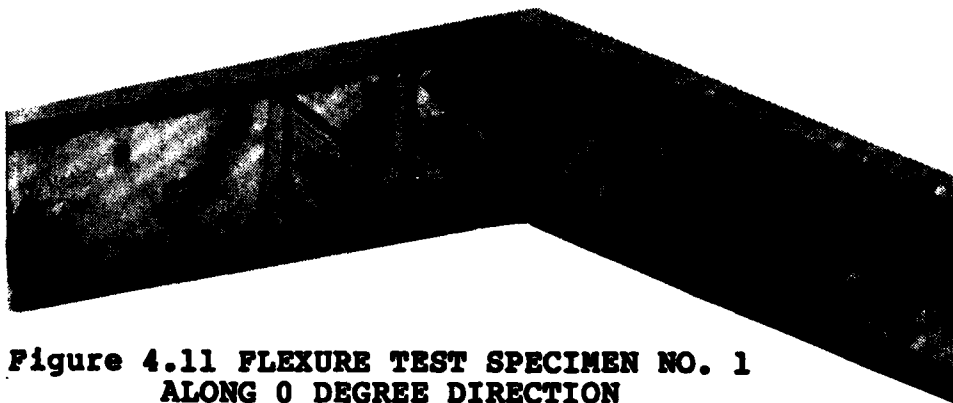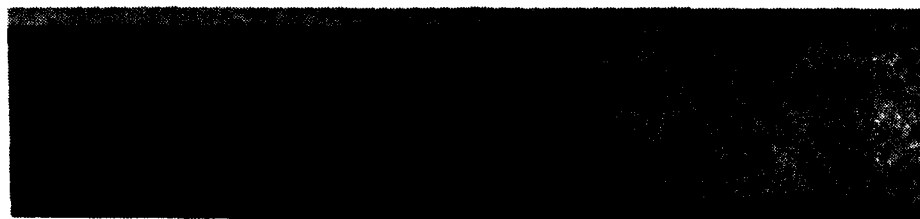
Figure 4.11 FLEXURE TEST SPECIMEN NO. 1
ALONG 0 DEGREE DIRECTION
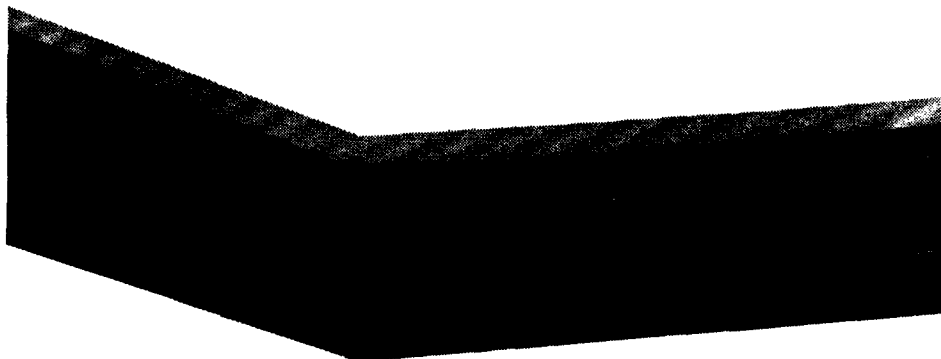
Figure 4.12 FLEXURE TEST SPECIMEN NO. 9
ALONG 90 DEGREE DIRECTION

Following the test program, failed test samples were taken back to the laboratory and x-rayed to determine if incipient failures could be observed. The x-ray negatives were made at transmission angles to show separations and none were observed. Any new separations resulting from deformation, if they existed, were too small for x-ray observation. It is suspected from surface shear bands that there were probably small separations from the cores internal to the structure. These however would coincide with natural changes in density and would be difficult to observe.

5.0 RESULTS AND RECOMMENDATIONS

The experimental program demonstrated the potential for an integration of the vehicle structure with the warhead to use the structural weight as deliverable fragment mass and to use the fragment mass to increase the structural strength and stiffness. The experimental strength measurements showed strengths approaching the maximum possible for the skin membrane of the integrated structure and far in excess of that from the skin in compression. In flexure, the multilayer fragments construction was equivalent to a solid beam (on a per unit length basis) of 70 % the fragment structure. This suggests that a structure composed of 20 gm fragments (2.54 cm or 1 in thick) will be equivalent in static strength to a sheet of steel 1.6 cm (5/8 in) thick. and a 60 gm fragment structure would have the same static strength as a solid steel structure 2.2 cm (7/8 in) thick. It is not possible to predict the strength of these structures as it depends on the skin thickness which in turn depends on the design of the warhead explosive.

The skin thickness selected for these experiments was approximately 0.23 cm (.090 in) as a nominal value. In an actual warhead the skin thickness would be the optimum to achieve fragmentation and fragment velocity following initiation of the explosive. When compared to skin thickness of other warheads made up of external and internal cans welded together to contain loose fragments the skin thickness is expected to be larger than the 0.23 cm (.090 in) and thus the strength is expected to be greater than that measured during this experimental program.

When the results in this study are compared to the current and advanced structures involving aluminum, graphite composites, or metal matrix composites, the potential for integration is apparent. The combination of warhead fragments and structure will reduce the sophistication required of the structural design because of the excess structural margin of the 1.5 cm (0.6 in.) thick structure. In a metal or composite skin construction the outer diameter and modulus provides the body stiffness required for guidance and control. In current systems this skin will be approximately 2.5 mm thick or less, depending on the sophistication of the design. However, the skin in conventional structural concepts must be compromised by adding weight in the form of thickness to provide inplane stiffness or buckling resistance for the blast considerations, and thick transition regions must be added for the joints. For the multilayer fragmenting integrated warhead structure this is the body stiffness is provided by the outer fragment skin (0.25 cm above) and the fragments which was not taken advantage of in any other design.

This is compounded to the benefits already achievable by not having to penetrate the conventional skin with the internal fragments.

This experimental program did show potential benefits to justify proceeding to determine experimentally how the fragmentation would occur in a simulated explosive warhead. The tensile specimen shown in Figure 4.4 shows the shear banding which should occur in tension if the fragments are to break apart cleanly. However, the fragment distribution in time and space needs to be determined before adequate trade studies can be made comparing this concept to others that are available.

If the explosive fragmentation results are as positive as these structural results this multilayer fragmenting integrated warhead structure is a design asset to future intercepter concepts. It can provide the structural stiffness in the outer structure needed by large or long structures or it can increase the volume of a small vehicle by exploding into a cloud of fragments on approaching a target.

APPENDIX I

CORE DIMENSIONAL CHARACTERISTICS

COMPOSITE DIMENSIONS

FRAGMENT MASS GM.	TETRAHEDRA UNIT SIZE IN.	OCTAHEDRAL UNIT SIZE IN.	COMPOSITE THICKNESS IN.	OCTAHEDRA HEIGHT IN.
5	.6923498	.5495311	.5653012	.3880652
10	.8722859	.6923498	.7122184	.4889202
15	.9985046	.7925319	.8152756	.5596664
20	1.098986	.8722859	.8973183	.6159866
25	1.183838	.9396345	.9665996	.6635466
30	1.258008	.9985046	1.027159	.7051191
35	1.324332	1.051147	1.081312	.7422939
40	1.384604	1.098986	1.130524	.7760766
45	1.440040	1.142987	1.175788	.8071490
50	1.491508	1.183838	1.217811	.8359970
55	1.539649	1.222048	1.257118	.8629803
60	1.584954	1.258008	1.294110	.8883739
65	1.627807	1.292021	1.329099	.9123931
70	1.668515	1.324332	1.362336	.9352101
75	1.707327	1.355138	1.394027	.9569647
80	1.744451	1.384604	1.424338	.9777726
85	1.780058	1.412866	1.453411	.9977307
90	1.814295	1.440040	1.481366	1.016921
95	1.847286	1.466226	1.508303	1.035412
100	1.879139	1.491508	1.534310	1.053266
105	1.909947	1.515961	1.559465	1.070534
110	1.939791	1.539649	1.583833	1.087262
115	1.968745	1.562630	1.607473	1.103490
120	1.996871	1.584954	1.630438	1.119255
125	2.024226	1.606666	1.652773	1.134588
130	2.050861	1.627807	1.674521	1.149517
135	2.076821	1.648412	1.695717	1.164068
140	2.102148	1.668515	1.716397	1.178264
145	2.126879	1.688144	1.736589	1.192125
150	2.151048	1.707327	1.756323	1.205672
200	2.367512	1.726089	1.933065	1.218921
300	2.710088	1.894668	2.212777	1.337967

APPENDIX II

SURROGATE BENDING TEST DATA

TABLE AII-1

SAMPLE CONFIGURATION	SPAN CM (IN)	LOAD LB.	LOAD KG.	DEFLECTION RANGE (.001 IN)			
				EDGE 1 THICKNESS=0.930		EDGE 2 THICKNESS=0.926	
				ORIG.	NORM.	ORIG.	NORM.
SOLID STANDARD 2.13 in WIDE	20.3 (8)	130.6	59.3	12.5	16.0	10.5	18.1
SOLID STANDARD 2.13 in WIDE	20.3 (8)	100.1	45.4	9.4	12.9	12.8	15.8
SOLID STANDARD 2.13 in WIDE	20.3 (8)	69.3	31.5	5.6	9.1	16.8	11.8
SOLID STANDARD 2.13 in WIDE	20.3 (8)	38.3	17.4	1.2	4.7	22.1	6.5
SOLID STANDARD 2.13 in WIDE	20.3 (8)	7.3	3.3	-3.5	0.0	28.6	0.0

FIGURE AII-1

SOLID STANDARD 8 in. SPAN

AII-1

TABLE AII-2

SAMPLE CONFIGURATION	SPAN CM (IN)	LOAD LB.	LOAD KG.	DEFLECTION RANGE (.001 IN)			
				EDGE 1 THICKNESS=0.930		EDGE 2 THICKNESS=0.926	
				ORIG.	NORM.	ORIG.	NORM.
SOLID STANDARD 2.13 in WIDE	20.3 (8)	161.4	73.3	14.2	12.5	0.0	
SOLID STANDARD 2.13 in WIDE	20.3 (8)	130.6	59.3	11.8	10.1	0.0	
SOLID STANDARD 2.13 in WIDE	20.3 (8)	100.1	45.4	8.6	6.9	14.0	6.8
SOLID STANDARD 2.13 in WIDE	20.3 (8)	69.3	31.5	5.9	4.2	11.6	4.4
SOLID STANDARD 2.13 in WIDE	20.3 (8)	38.3	17.4	1.7	0.0	7.2	0.0

FIGURE AII-2

SOLID STANDARD 8 in. SPAN

AII-2

TABLE AII-3

SAMPLE CONFIGURATION (3.42 in WIDE)	SPAN CM (IN)	LOAD LB.	LOAD KG.	DEFLECTION RANGE (.001 IN)			
				EDGE 1 THICKNESS=1.07		EDGE 2 THICKNESS=1.07	
				ORIG.	NORM.	ORIG.	NORM.
060 SKIN 90 DEG.	20.3 (8)	161.4	73.3	13.6	9.9	14.0	8.5
060 SKIN 90 DEG.	20.3 (8)	130.6	59.3	11.9	8.2	13.2	7.7
060 SKIN 90 DEG.	20.3 (8)	100.1	45.4	9.7	6.0	11.1	5.6
060 SKIN 90 DEG.	20.3 (8)	69.3	31.5	6.9	3.2	8.6	3.1
060 SKIN 90 DEG.	20.3 (8)	38.3	17.4	3.7	0.0	5.5	0.0

FIGURE AII-3

0.060 SKIN 90° DIRECTION 8 in SPAN

AII-3

TABLE AII-4

SAMPLE CONFIGURATION (2.8 in. WIDE)	SPAN CM (IN)	LOAD LB.	LOAD KG.	DEFLECTION RANGE (.001 IN)			
				EDGE 1 THICKNESS=1.06		EDGE 2 THICKNESS=1.08	
				ORIG.	NORM.	ORIG.	NORM.
060 SKIN 0 DEG.	15.24 (6)	161.4	73.3	20.5	14.5	22.7	15.9
060 SKIN 0 DEG.	15.24 (6)	130.6	59.3	17.8	11.8	19.5	12.7
060 SKIN 0 DEG.	15.24 (6)	100.1	45.4	14.5	8.5	15.6	8.8
060 SKIN 0 DEG.	15.24 (6)	69.3	31.5	10.4	4.4	11.7	4.9
060 SKIN 0 DEG.	15.24 (6)	38.3	17.4	6.0	0.0	6.8	0.0

FIGURE AII-4

0.060 SKIN 0° DIRECTION 6 in. SPAN
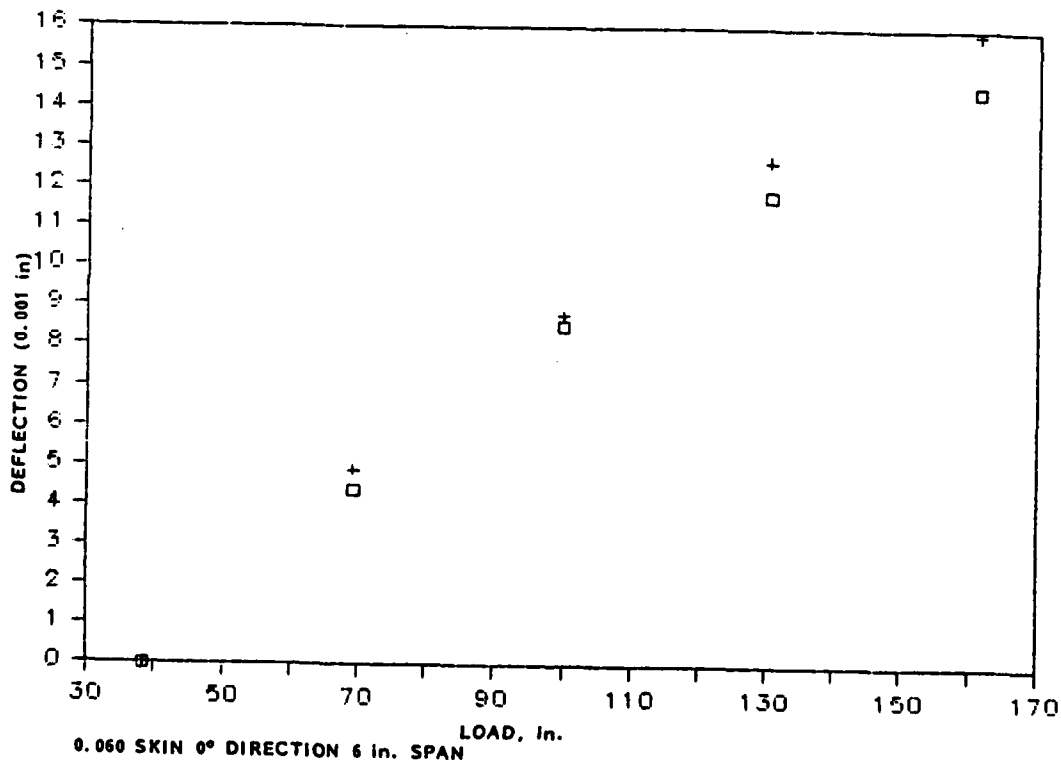
TABLE AII-5

SAMPLE CONFIGURATION (2.8 in WIDE)	SPAN CM (IN)	LOAD LB.	LOAD KG.	DEFLECTION RANGE (.001 IN)			
				EDGE 1 THICKNESS=1.06		EDGE 2 THICKNESS=1.08	
				ORIG.	NORM.	ORIG.	NORM.
060 SKIN 0 DEG.	20.3 (8)	130.6	59.3	20.5	18.5	13.3	15.7
060 SKIN 0 DEG.	20.3 (8)	100.1	45.4	17.2	15.2	10.6	13.0
060 SKIN 0 DEG.	20.3 (8)	69.3	31.5	13.2	11.2	8.0	10.4
060 SKIN 0 DEG.	20.3 (8)	38.3	17.4	3.6	1.6	2.8	5.2
060 SKIN 0 DEG.	20.3 (8)	7.3	3.3	2.0	0.0	-2.4	0.0

FIGURE AII-5

0.060 SKIN 0° DIRECTION 8 in. SPAN
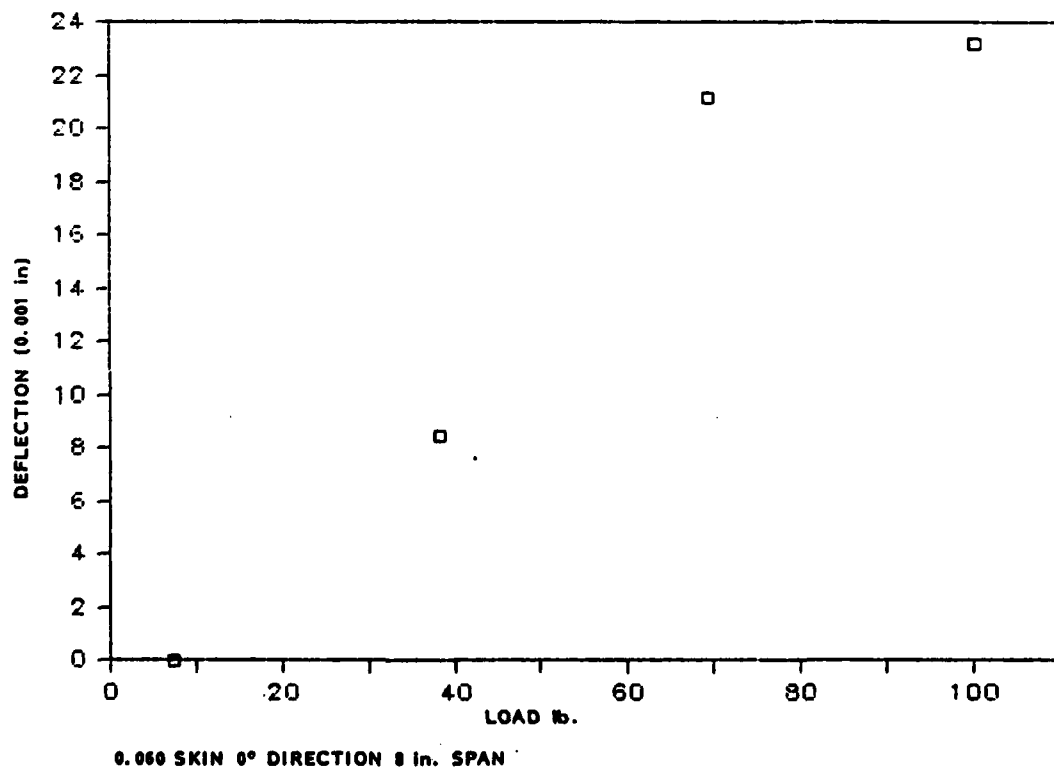
TABLE AII-6

SAMPLE CONFIGURATION (2.1 in WIDE)	SPAN CM (IN)	LOAD LB.	LOAD KG.	DEFLECTION (.001 IN) EDGE 1 THICKNESS=0.912	
				ORIG.	NORM.
030 SKIN 0 DEG.	15.24 (6)	100.1	45.4	0.1	9.0
030 SKIN 0 DEG.	15.24 (6)	69.3	31.5	-4.5	4.4
030 SKIN 0 DEG.	15.24 (6)	38.3	17.4	-8.9	0.0

FIGURE AII-6
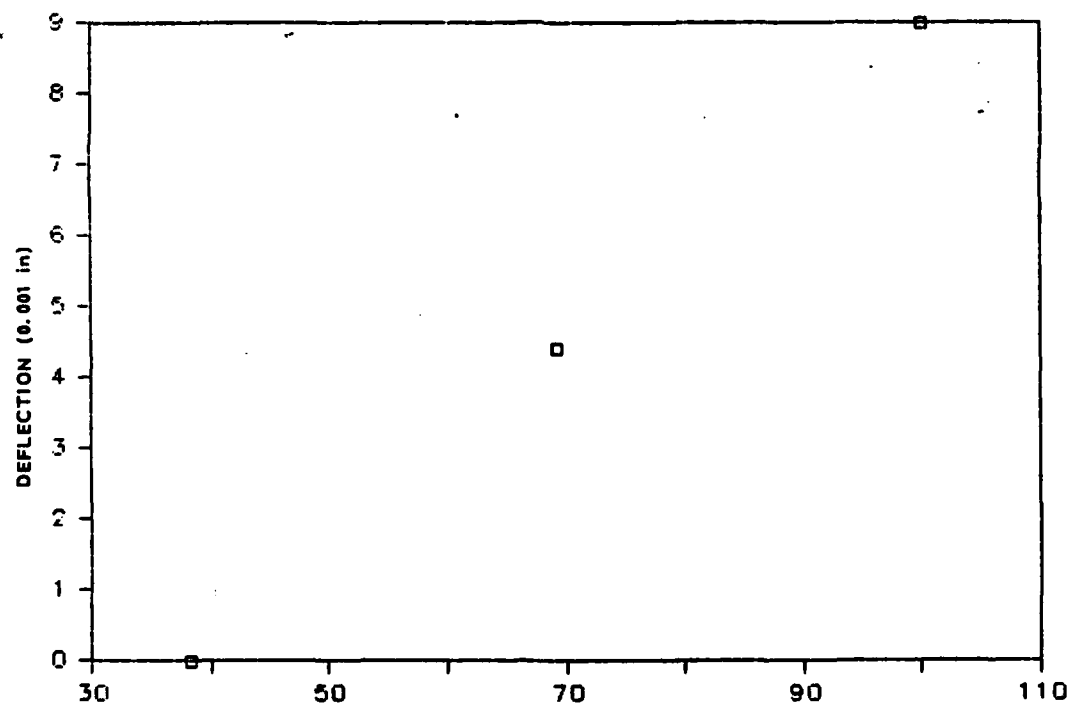
0.030 SKIN 0° DIRECTION 6 in SPAN

AII-6

DISTRIBUTION LIST

No. of Copies

Office of Deputy Under Secretary of Defense
for Research and Engineering (ET)
ATTN: Mr. J. Persh, Staff Specialist for Materials   1
       and Structures (Room 3D1089)
The Pentagon
Washington, DC 20301

Office of Deputy Chief of Research Development
and Acquisition
ATTN: DAMA-CSS   1
The Pentagon
Washington, DC 20301

Commander
U.S. Army Materiel Command
ATTN: AMCLD, R. Vitali, Office of Laboratory Management   1
5001 Eisenhower Avenue
Alexandria, VA 22333

Director
Ballistic Missile Defense Systems Command
ATTN: BMDSC-TEN, N. J. Hurst   1
      BMDSC-HE, J. Katechis   1
      BMDSC-HNS, R. Buckelew   1
      BMDSC-AOLIB   1
P.O. Box 1500
Huntsville, AL 35807

Director
Ballistic Missile Defense Advanced Technology Center
ATTN: ATC-X, D. Russ   1
      ATC-X, Col. K. Kawano   1
      ATC-M, D. Harmon   1
      ATC-M, J. Papadopoulos   1
      ATC-M, S. Brockway   1
P.O. Box 1500
Huntsville, AL 35007-3801

Director
Defense Nuclear Agency
ATTN: SPAS,   1
Washington, DC 20305

Director
Army Ballistic Research Laboratories
ATTN: DRDAR-BLT, Dr. N. J. Huffington, Jr.   1
      DRDAR-BLT, Dr. T. W. Wright   1
      DRDAR-BLT, Dr. G. L. Moss   1
Aberdeen Proving Ground, MD 21005

Commander
Harry Diamond Laboratories
ATTN: DRXDO-NP, Dr. F. Wimenitz   1
2800 Powder Mill Road
Adelphi, MD 20783

Commander
Air Force Materials Laboratory
Air Force Systems Command
ATTN: LNC/Dr. D. Schmidt   1
Wright Patterson Air Force Base
Dayton, OH 45433

Commander
BMO/ABRES Office
ATTN: BMO/MNRT, Col. R. Smith   1
Norton Air Force Base, CA 92409

Commander
Air Force Materials Laboratory
ATTN: AFML/MBM, Dr. S. W. Tsai   1
Wright-Patterson Air Force Base
Dayton, OH 45433

Commander
Naval Ordinance Systems Command
ATTN: ORD-03331, Mr. M. Kinna   1
Washington, DC 20360

Naval Postgraduate School
ATTN: Code NC4(67WT),
      Professor E. M. Wu   1
Monterey, CA 93943

Commander
Naval Surface Weapons Center
ATTN: C. Lyons   1
      C. Rowe   1
Silver Springs, MD 20910

Lawrence Livermore Laboratory
ATTN: W. Hubbel   1
P.O. Box 808 (L-122)
Livermore, CA 94550

Sandia Laboratories
ATTN: Dr. L. D. Bertholf   1
      Dr. J. Lipkin   1
P.O. Box 5800
Albuquerque, NM 87115

Aerospace Corporation
ATTN: Dr. R. Cooper   1
P.O. Box 92957
Los Angeles, CA   90009

AVCO Corporation
Government Products Group
ATTN: Dr. W. Reinecke   1
        P. Rolincik   1
201 Lowell Street
Wilmington, MA   01997

ETA Corporation
ATTN: D. L. Mykkanen   1
P.O. Box 6625
Orange, CA   92667

Fiber Materials, Inc.
ATTN: M. Subilia, Jr.   1
        L. Landers   1
        R. Burns   1
Biddeford Industrial Park
Biddeford, ME   04005

General Electric Company
Advanced Materials Development Laboratory
ATTN: K. Hall   1
        J. Brazel   1
3198 Chestnut Street
Philadelphia, PA   19101

General Dynamics Corporation
Convair Division
ATTN: J. Hertz   1
5001 Kearny Villa Road
San Diego, CA   92138

General Research Corporation
ATTN: Dr. R. Wengler   1
        Dr. R. Parisse   1
        J. Green   1
5383 Hollister Avenue
Santa Barbara, CA   93111

Kaman Sciences Corporation
ATTN: Dr. D. Williams   1
P.O. Box 7463
Colorado Springs, CO   80933

Ktech
ATTN: Dr. D. Keller   1
911 Pennsylvania Avenue, N.E.,
Albuquerque, NM 87110

Lehigh University
Institute of Fracture and Solid Mechanics
ATTN: Dr: George C. Sih   1
Bldg. 39, Packard Lab
Bethlehem, PA 18015

Los Alamos National Laboratory
ATTN: Henry L. Horak   1
Mail Stop C936
Los Alamos, NM 87545

Martin Marietta Aerospace
ATTN: V. Hewitt   1
      Frank H. Koo   1
P.O. Box 5837
Orlando, FL 32805

Pacifica Technology, Inc.
ATTN: Dr. Ponsford   1
P.O. Box 148
Del Mar, CA 92014

Radkowski Associates
ATTN: Dr. P. Radkowski   1
P.O. Box 5474
Riverside, CA 92507

Southwest Research Institute
ATTN: A. Wenzel   1
8500 Culebra Road
San Antonio, TX 78206

Terra Tek, Inc.
ATTN: Dr. A. H. Jones   1
420 Wakara Way
Salt Lake City, UT 84108

Defense Documentation Center   1
Cameron Station, Bldg. 5
5010 Duke Station
Alexandria, VA 22314

4

Director
Army Materials and Mechanics Research Center
ATTN: AMXMR-B, J. F. Dignam   1
        AMXMR-B, Dr. S. C. Chou   5
        AMXMR-B, L. R. Aronin   1
        AMXMR-B, Dr. D. P. Dandekar   1
        AMXMR-K   1
        AMXMR-PL   2
Watertown, MA 02172

Army Materials and Mechanics Research Center
Watertown, Massachusetts 02172
DEVELOPMENT AND CHARACTERIZATION OF
MULTILAYER INTEGRATED WARHEAD STRUCTURE
D. L. NYKRANEN
ETA CORPORATION
P. O. Box 6625
Orange, CA 92667

Technical Report AMMRC TR 85-16, MAY 1985, 38 pp.
D/A Project: 8X363304D215 Contract DAAG46-83-C-0167
AMCMS CODE: P493000.215
Final Report, March 83 to September 84

Key Words
Warheads
Fragmentation
Investment casting
Tensile strength
Structural elements

This experimental program demonstrated the potential benefits from an integrated multilayered fragmenting warhead structure which uses the structural weight as deliverable fragment mass to increase the structural strength and stiffness. The fabrication techniques and design developments were accomplished using war and polyester as surrogates for the ceramic cores and cast steel of the final concept. Steel castings (17-4PH) were made and specimens were machined to characterize the structural properties of the concept. The property measurements showed tensile strengths approaching the maximum possible for an annealed cast steel skin. The compressive strengths were greater than that expected for the skin membrane of the integrated structure. In flexure, the multilayer fragments construction was equivalent to a solid beam (on a per unit length basis) 70% the thickness of fragment structure. The shear banding found in the tensile specimens suggests a potential for fragmentation under explosive loading and justifies continuing to characterize the concept.

END

FILMED

9-85

DTIC